

Partitioning two-dimensional mixed phase spaces

Kevin A. Mitchell

School of Natural Sciences, University of California, Merced, California, 95344

Abstract

Hamiltonian systems typically exhibit a mixture of chaos and regularity, complicating any scheme to partition phase space and extract a symbolic description of the dynamics. In particular, the dynamics in the vicinity of stable islands can exhibit complicated topology that is qualitatively distinct from that away from the islands. We develop an approach to partition the chaotic phase space of a general dynamical system represented by a two-dimensional map (homeomorphism). This approach can accommodate mixed phase space structure with an arbitrarily high degree of accuracy. The partitioning scheme is built around networks of nested heteroclinic tangles – fundamental geometric objects that organize phase space transport. These tangles can be used to progressively approximate the dynamics in the vicinity of stable island chains. The net result is a symbolic approximation to the dynamics in the chaotic sea, and an associated phase-space partition, which includes the influence of stable islands and which is approximately Markov.

Keywords: partitions, homoclinic and heteroclinic tangles, symbolic dynamics, chaotic transport, mixed phase space

1. Introduction

This paper develops a general strategy for partitioning the phase space of a dynamical system specified by a map (homeomorphism) on a two-dimensional phase space. In physical applications, such maps often arise either as the time-advance map of a periodically forced Hamiltonian or as the Poincaré return map defined on a surface of section for an autonomous Hamiltonian. Though we have in mind Hamiltonian systems, for which the maps are area preserving, area preservation itself is not required for the present technique.

Partitions provide a powerful tool to analyze chaotic systems [1, 2]. Partitioning phase space into distinct regions leads to a discrete description of the dynamics—the current state of the system is described by the partition element in which it resides, rather than its precise location in phase space. By assigning a unique symbol to each such element, a trajectory of the original system can be assigned a symbolic itinerary. A “good” partition generates an equivalent (or nearly equivalent) representation of the original dynamics in terms of a shift map on the symbolic itineraries. For many problems, the study of the symbolic representation, i.e. the itineraries and associated shift map, is easier than the original representation of the dynamics [2]. For example, a symbolic representation greatly simplifies the task of counting, labeling and classifying the periodic, heteroclinic, and other chaotic orbits; it helps in studying the fractal properties of the dynamics; and it allows the direct computation of rigorous bounds on topological entropy.

Explicit partitions have numerous other practical benefits. As one example, they are useful tools for finding periodic orbits, which themselves have a host of applications to both classical

and quantum dynamics [3, 4]. A typical strategy for finding a periodic orbit begins with an accurate initial guess, which is then refined by Newton’s method; partitions are useful for constructing the initial guess. As a second example, partitions provide a basis to approximate the Frobenius-Perron operator following Ulam’s method [5, 6], from which escape rates, Lyapunov exponents, and invariant measures can be computed.

Despite their utility, in practice it is often not obvious how to explicitly construct a good partition. (See for example Ref. [7].) Though the simplest case of a one-dimensional map on an interval has been well studied using kneading theory [8, 9], for two-dimensional maps, the theory is less complete. The existence of Markov partitions is well established in the hyperbolic case [1], and a partitioning technique for the dissipative Henon map was introduced by Grassberger and Kantz [10, 11]. (See also the work on pruning [12].) However, in physical applications most Hamiltonian systems generate non-hyperbolic maps, which exhibit a mixture of regular motion (islands of stability) embedded within a chaotic sea. In such cases, much less is known. Important work toward this end are the papers of Christiansen and Politi [13, 14, 15] and Jung and Emmanouilidou [16]. A primary reason for the difficulty encountered in mixed phase spaces is that the dynamics in the vicinity of the stable islands can be radically different from that away from the islands.

This paper describes a technique to construct phase space partitions that is flexible enough to accommodate the influence of stable islands on the dynamics within the surrounding chaotic sea. The accuracy of the partition can be systematically refined to include arbitrarily fine-scale structure, either near the islands or anywhere else in phase space. At any stage of resolution, the partition provides a Markov model to the dynamics within the chaotic sea, in the sense that there is an associated Markov shift with the property that every allowed itinerary of

Email address: kmitche11@ucmerced.edu (Kevin A. Mitchell)

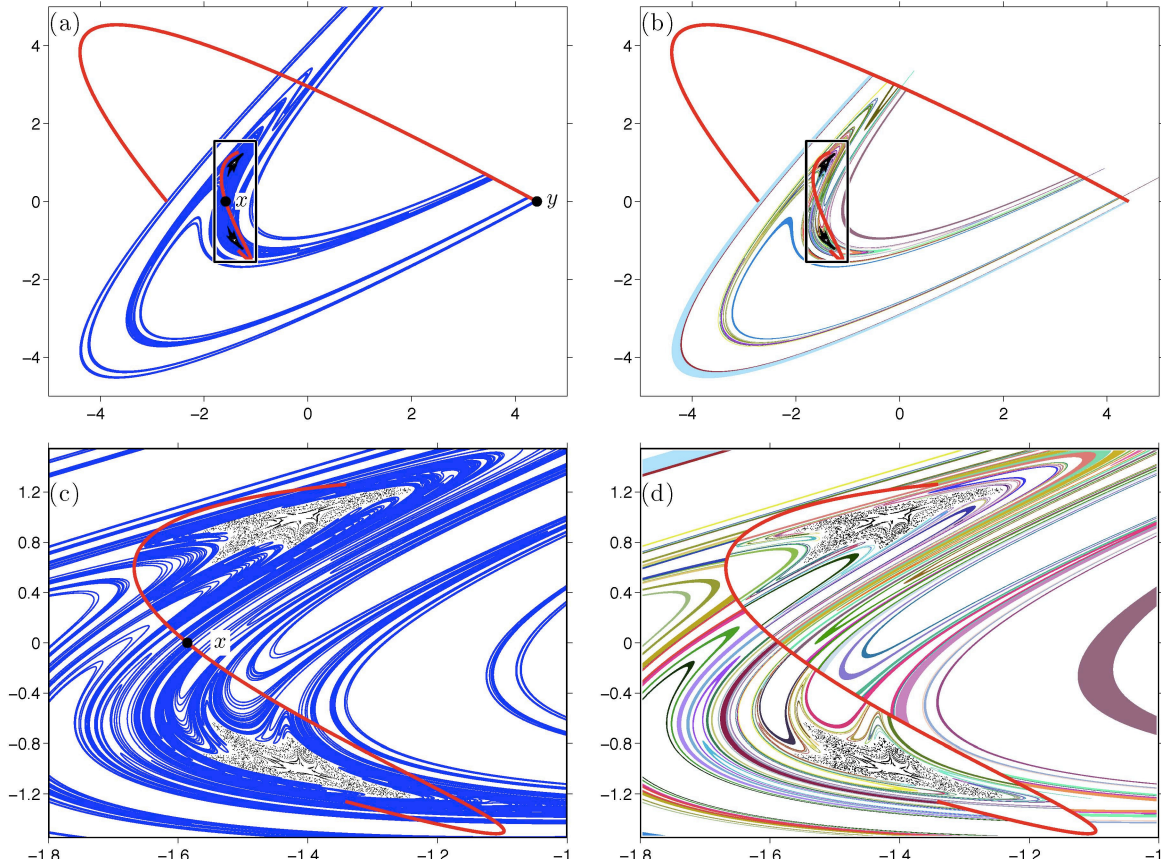


Figure 1: (Color online) Figure 1a shows a trellis (finite-length stable and unstable intervals) for a member of the area-preserving Henon family of maps. Figure 1c shows an expanded view of the black rectangle. This expansion highlights the period-two island chain and surrounding tangle attached to the central fixed point x . Figure 1b shows the partition constructed from the manifolds in Fig. 1a, with each partition domain shaded a randomly chosen color. Figure 1d shows an expanded view of the partition in the vicinity of the stable islands. There are a total of 114 domains in the partition.

the shift corresponds to (at least) one trajectory of the original dynamical system.

Figure 1 shows an example drawn from the area-preserving Henon family. The left column shows finite-length intervals of stable and unstable manifolds attached to two fixed points x and y . (Fig. 1c is an expansion of the black box in Fig. 1a.) The stable intervals are the two thick, red curves. The unstable intervals are the thin, blue curves, which explore a large region of phase space with considerable density. The topological structure of the stable and unstable manifolds, in terms of how they intersect and how these intersections map forward, encodes considerable information about the topology of the dynamics. Using the methods presented here, this information allows us to construct the partition shown in the right column of Fig. 1, where each domain of the partition is shaded with a randomly chosen color. The primary purpose of this paper is to explain this construction, i.e. how the partition on the right can be constructed from the information stored in the curves on the left.

The dynamics in Fig. 1a contains a period-two stable island chain, most easily seen by the ensemble of black points in Fig. 1c. Note in Fig. 1d that the partition domains extend into the region immediately surrounding the islands, meaning

that the dynamics in the vicinity of the islands is incorporated into the partition construction. The reason we are able to do this is that the unstable manifolds in Fig. 1c themselves explore the vicinity of the islands. In fact, we have utilized the stable and unstable manifolds attached to the central fixed point x of Fig. 1c to specifically target this region. Typically, within the vicinity of a stable island chain, we can extract information about the local dynamics by computing the heteroclinic tangle attached to unstable periodic points lying between the individual islands.

This paper builds on our prior studies [17, 18, 19] of the topology of networks of heteroclinic tangles and the symbolic dynamics encoded by them. An independent approach to this problem has also been developed by Collins [20, 21, 22, 23, 24]. Both approaches present algorithms to extract symbolic dynamics from tangles without ever introducing a partition. In the case of Refs. [17, 18, 19], symbolic dynamics is cast in terms of homotopy theory, focusing on how curves, rather than domains, map forward. In the case of Refs. [20, 21, 22, 23, 24], symbolic dynamics is based on the theory of train tracks and the Bestvina-Handel algorithm [25, 26]. Additional topological studies of tangles can be found in Refs. [27, 28, 29, 30, 31, 32, 33, 16].

The present work should be distinguished from set-oriented

methods [34], which also partition phase space into domains, typically simple rectangular cells on a regular, though possibly refined, grid. Such set-oriented techniques emphasize the measure-theoretic aspects of transport. The objective here is to develop topologically relevant partitions yielding an approximately Markov symbolic dynamics.

This paper is structured as follows. Section 2 summarizes the key results of the homotopic lobe dynamics technique developed in Ref. [17]. Section 3 introduces the concept of “robust distorted bridges”, or RoD-bridges. These are unstable intervals needed in the construction of the partition rectangles. The RoD-bridges have a natural ordering, which is discussed in Sec. 4. Section 5 then explains how the partition rectangles are constructed from supremum and infimum intervals of this ordering. Section 6 introduces symbolic itineraries for the RoD-bridges, and Sec. 7 shows how the ordering of RoD-bridges can be computed from their itineraries. Finally, in Sec. 8, the itineraries of the intervals bounding the partition rectangles are constructed. This final step allows the partition rectangles to be explicitly computed. An example is worked out in Sec. 9. Section 10 contains concluding remarks.

2. Homotopic Lobe Dynamics

The theory of homotopic lobe dynamics is a method of extracting symbolic dynamics from finite-length intervals of stable and unstable manifolds. As initially developed, the theory makes no use of phase space partitions. We summarize here the main points of the theory (following Ref. [17]), before explaining in subsequent sections how it leads to a partitioning scheme.

2.1. The initial trellis T

In this paper, the dynamics is specified by a map M defined on a subdomain of the plane. (Specifically, M is assumed to be a homeomorphism.) We then consider a heteroclinic ¹ tangle W of M [35]. The tangle W consists of the one-dimensional stable and unstable manifolds, denoted W^S and W^U , that are attached to some set of unstable periodic orbits, denoted P . We call P the set of *anchor points*. Though the stable and unstable manifolds of P do not self-intersect [35], they can and typically do intersect one another, forming a complicated pattern of criss-crossing curves that justifies the name tangle. Since these manifolds are infinitely long, we consider only the information contained in a finite-length truncation, which we call a trellis, following Collins [20, 21, 36, 22, 23, 24]. ²

Definition 1 (trellis). A trellis T consists of a finite set P of unstable periodic orbits, which we call the anchor points, together with subsets T^S and T^U of the stable and unstable manifolds

¹Since there is no common term that includes both homoclinic and heteroclinic, we use heteroclinic as a generic term here, encompassing both homoclinic and heteroclinic.

²Our use of “trellis” differs subtly from that of Rom-Kedar [29, 30], who uses the term “trellis” for a complete tangle W , with infinitely long manifolds, that is described by a finite amount of information.

W^S and W^U of P , where T^S and T^U are each the union of a finite number of compact subintervals (of nonzero length), and where $M(T^S) \subset T^S$ and $M(T^U) \supset T^U$.

In practice, the trellis is almost always computed numerically, often guided by some initial knowledge or intuition about the phase space structure.

The full tangle W is generated by infinitely many iterations of the trellis T , i.e. $W^U = \cup_{n \geq 0} M^n(T^U)$ and $W^S = \cup_{n \leq 0} M^n(T^S)$. It is important to emphasize, however, that the trellis T is fixed at the beginning of this analysis, and all subsequent analysis is based on the topological information contained in T . Though the construction of the partition may necessitate the use of intervals contained in W but not T , as we shall discuss in detail later, the prescription for constructing the partition is based solely on the topological information in T . (For example, the topological entropy of the transition matrix for the partition can be computed from T .)

We define W_z^S to be the connected component of W^S containing the periodic point $\mathbf{z} \in P$, and we define $T_z^S = T^S \cap W_z^S$. We define W_z^U and T_z^U analogously. We use $W^S[\mathbf{p}, \mathbf{q}]$ for the closed interval of W^S between two points $\mathbf{p}, \mathbf{q} \in W^S$ and similarly $W^S(\mathbf{p}, \mathbf{q})$, $W^S[\mathbf{p}, \mathbf{q})$, $W^S(\mathbf{p}, \mathbf{q}]$ for the corresponding open and half-open intervals. Analogous notation is used for W^U , T^S , and T^U .

A stable *branch* of W is an interval $B_z^S = W^S[\mathbf{z}, \infty)$ that has one endpoint anchored at $\mathbf{z} \in P$ and that extends away from \mathbf{z} for an infinite arc length along W^S . An unstable branch $B_z^U = W^U[\mathbf{z}, \infty)$ is defined analogously. Each stable or unstable branch B_z has a minimum period p such that $M^p(B_z) = B_z$. Clearly, the period of the point \mathbf{z} must divide the period of the branch B_z . Finally, a branch of the trellis T is defined as the intersection between T and a branch of the tangle W .

We require that T satisfy the following further conditions.

1. **Connectedness Condition** Every stable branch B_z^S of T^S consists of a *single* compact interval of W^S . We denote the endpoints of T^S that are not in P by the set N (for Nonperiodic).
2. **Alternating Branches Condition** For each periodic point $\mathbf{z} \in P$, an equal (and nonzero) number of stable and unstable branches of T are attached to \mathbf{z} , alternating between stable and unstable as one encircles \mathbf{z} .
3. **Primary Intersection Condition** Each unstable branch B_z^U of T^U contains a unique point $\mathbf{p} \in N$. Furthermore, $T^U(\mathbf{z}, \mathbf{p}) \cap T^S = \emptyset$, i.e. the (open) unstable interval connecting \mathbf{z} to \mathbf{p} does not intersect any of the stable branches of the trellis.
4. **Endpoint Condition** For any endpoint \mathbf{x} of a connected component of T^U , its preiterate $M^{-1}(\mathbf{x})$ must lie in $T^S \setminus N$.
5. **Transversality Condition** Any trellis intersection $T^S \cap T^U$ that is not an endpoint of T^U is topologically transverse, i.e. at such an intersection point, T^U passes locally from one side of T^S to the other side of T^S .

One consequence of these conditions is that all endpoints of T^U lie in T^S , and all endpoints of T^S lie in T^U . Also, the Primary Intersection Condition implies that each point in N is a

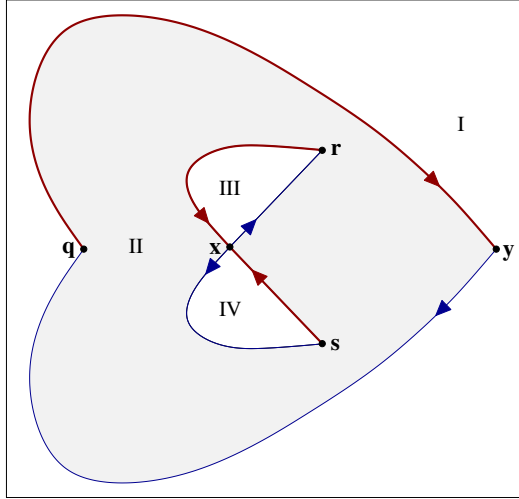


Figure 2: (Color online) The above is a simplified version of Fig. 1a, illustrating the four zones defined by the trellis. The points $\mathbf{x}, \mathbf{y} \in P$ are fixed points and $\mathbf{q}, \mathbf{r}, \mathbf{s} \in N$ are pips. The stable intervals in T^S and the unstable intervals in $\hat{T}^U = \cup\{T^U[\mathbf{z}, \mathbf{p}]\mid \mathbf{z} \in P, \mathbf{p} \in N\}$ divide the plane into the four zones I, II, III, and IV. Thick (red) curves are stable segments and thin (blue) curves are unstable segments, a convention we use throughout the paper.

primary intersection point, or pip, as defined by Rom-Kedar and Wiggins [37]³. As discussed in Ref. [17], the Alternating Branches and Transversality Conditions can be relaxed somewhat.

We call an initial trellis interval $T^U[\mathbf{z}, \mathbf{p}]$, connecting an anchor point $\mathbf{z} \in P$ to a pip $\mathbf{p} \in N$, an *anchor interval* (or *anchor bridge*, see Sec. 2.3). The collection of all anchor intervals is denoted $\hat{T}^U = \cup\{T^U[\mathbf{z}, \mathbf{p}]\mid \mathbf{z} \in P, \mathbf{p} \in N\}$. The anchor intervals together with the stable intervals in T^S divide the plane into disjoint regions called *zones*. See Fig. 2 for an illustration.

Example: We shall illustrate the concepts in this paper using the same example map used in Ref. [17], which is a surface-of-section map defined for a hydrogen atom in applied parallel electric and magnetic fields [38, 39]. [Following Ref. [17], the electron energy is $E = 0.5$ and the magnetic field strength is $B = 2.141$, in scaled units.] Figure 3a shows the trellis, and Fig. 3b is a qualitative rendering showing the topology of the unstable manifold more clearly. The trellis has a single stable and unstable branch, with $P = \{\mathbf{z}\}$ and $N = \{\mathbf{p}_0\}$. The stable branch T^S and unstable interval $\hat{T}^U = W^U[\mathbf{z}, \mathbf{p}_0]$ divide the plane into two zones, the resonance zone and the external zone.

2.2. Homotopy

The key step in the topological analysis is to punch holes in the plane adjacent to judiciously selected heteroclinic points, called pseudoneighbors.

³A pip is an intersection point $\mathbf{p} \in W_{\mathbf{z}}^U \cap W_{\mathbf{z}'}^S$, with $\mathbf{z}, \mathbf{z}' \in P$, such that $W_{\mathbf{z}}^U(\mathbf{z}, \mathbf{p}) \cap W_{\mathbf{z}'}^S(\mathbf{z}', \mathbf{p}) = \emptyset$.

Definition 2 (pseudoneighbors). Defining $X = \cup_{n \in \mathbb{Z}} \{M^n(\mathbf{x}) \mid \mathbf{x} \in T^S \cap T^U\}$, two homo/heteroclinic intersection points $\mathbf{x}, \mathbf{x}' \in X$ are called a pair of pseudoneighbors (with respect to T) if \mathbf{x} and \mathbf{x}' lie on the same stable and unstable branches of W and if $W^S(\mathbf{x}, \mathbf{x}') \cap X = W^U(\mathbf{x}, \mathbf{x}') \cap X = \emptyset$.

In short, the stable and unstable (open) intervals connecting a pair of pseudoneighbors contain no trellis intersection nor any iterate of a trellis intersection. For a given pair of pseudoneighbors \mathbf{x} and \mathbf{x}' , we punch a hole inside the domain bounded by the stable and unstable intervals $W^S[\mathbf{x}, \mathbf{x}']$ and $W^U[\mathbf{x}, \mathbf{x}']$ connecting them. The hole is placed infinitesimally close to one of the two pseudoneighbors. (See Ref. [17] for details.)

The above definition implies that any iterate $\mathbf{x}_n = M^n(\mathbf{x}_0)$ of a pseudoneighbor is also a pseudoneighbor, meaning that each pseudoneighbor generates an entire orbit of pseudoneighbors. For each such orbit, the holes, likewise, are placed so as to form an orbit, i.e. the holes are arranged in bi-infinite sequences where each hole maps to another hole.

Example: In Figs. 3a and 3b, the “3” marks a pair of pseudoneighbors. The neighboring circle represents the associated hole. Mapping this hole forward and backward generates a bi-infinite sequence of holes associated with the pair of pseudoneighbor trajectories, converging upon \mathbf{z} in both forward and backward time.

In addition to holes next to pseudoneighbors, for technical reasons we also punch holes adjacent to the pips in N and their preiterates. Since these holes do not play a central role here, we refer to Ref. [17] for further discussion.

For a directed curve (or path) A that begins and ends on T^S and that does not intersect any hole, its homotopy class $[A]$ contains all directed curves obtained from continuously distorting A without passing through any hole and without removing the endpoints from T^S . Homotopy classes admit a natural multiplicative structure. If A ends on the same connected component of T^S that another curve B begins, then the product of classes $[A][B]$ is the homotopy class of the curve formed by A concatenated with B , where the final point of A is joined to the initial point of B by an interval of T^S . Furthermore, $[A]^{-1}$ is the homotopy class of the curve A with its direction reversed. Clearly $[A][A]^{-1}$ is trivial, meaning that any representative curve from this class is contractable to a point.

2.3. Bridge-classes

The unstable manifold W^U can be cut into intervals called *bridges*.

Definition 3 (bridge). A bridge is a closed interval of W^U that begins and ends on T^S , but does not otherwise intersect T^S .

Associated with bridges are the following homotopy classes.

Definition 4 (bridge-class). A bridge-class is the homotopy class of a directed curve B that forms a closed interval of W^U that begins and ends on T^S , and such that B can be homotopically deformed into a directed curve that only intersects T^S at the curve’s endpoints.

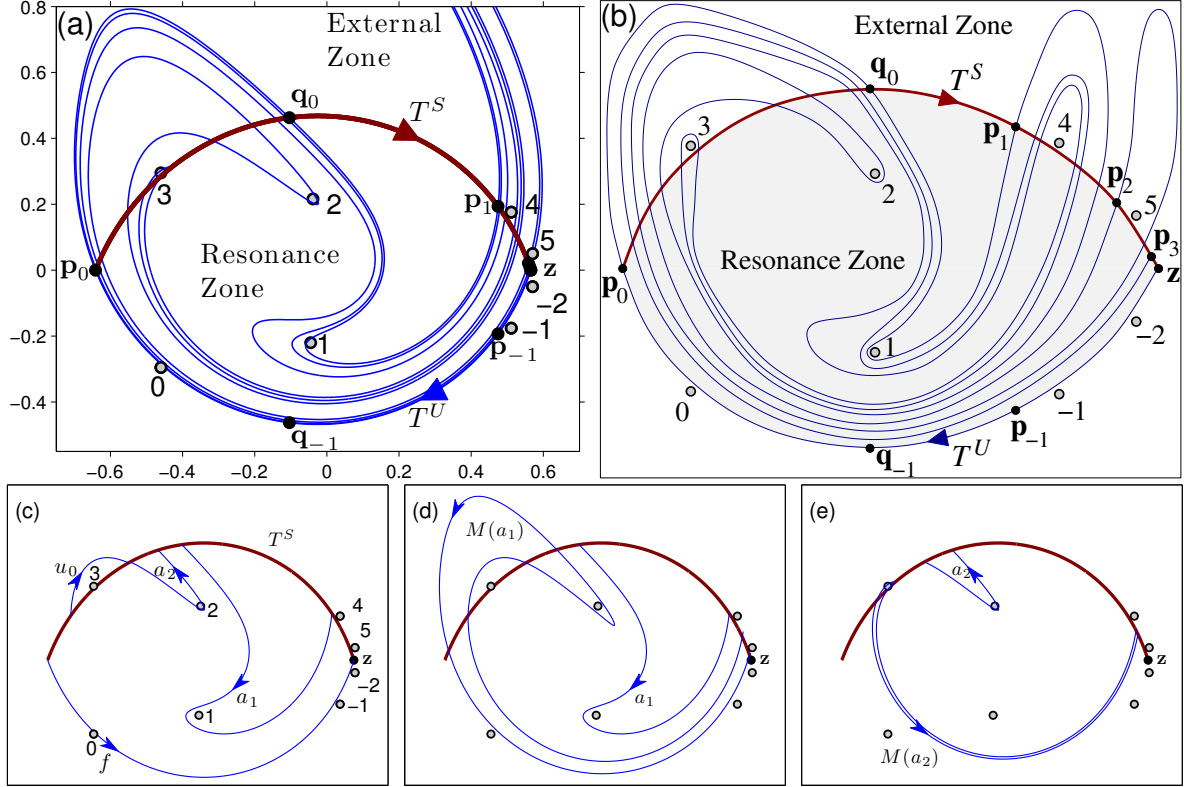


Figure 3: (Color online) Segments of the homoclinic tangle computed from the map defined in Ref. [39] for parameters $E = 0.5$ and $B = 2.141$. The thick (red) curves are stable segments and the thin (blue) curves are unstable segments. An unbarbed (triangular) arrow, as in Fig. 3a, denotes the natural dynamical order along the stable or unstable manifold. A barbed arrow, as in Fig. 3c, denotes the direction of a bridge-class. Shaded circles denote holes. (a) The initial trellis, from which the homotopic lobe dynamics will be extracted. (b) A qualitative depiction of Fig. 3a. The resonance zone is shaded. (c) Representative curves for the most important bridge-classes. (d) and (e) each shows a representative curve and its forward iterate.

Clearly, the homotopy class of a bridge is a bridge-class, but a bridge-class need not contain a bridge.

Example: Fig. 3c shows one representative bridge from each of four bridge-classes a_1 , a_2 , f , and u_0 . Classes a_1 and a_2 encircle holes 1 and 2, respectively, whereas f encircles both. The class u_0 encircles hole 3. Iterating u_0 forward generates an infinite sequence of classes u_0, u_1, u_2, \dots (only u_0 shown), encircling holes 3, 4, 5,

We should clarify here an important point about the orientations of unstable intervals. First, the dynamics naturally endows any stable or unstable interval with an orientation, or direction. For a stable interval, this direction points along the manifold toward the periodic point, whereas for an unstable interval, this direction points away. In the figures, this dynamical direction is denoted by unbarbed (triangular) arrows. However, if we consider an unstable interval as a representative curve of a bridge-class, it carries another direction, defined by the orientation of the class. This homotopy direction may or may not be equal to the dynamical direction. In the figures, the homotopy direction is distinguished by *barbed* arrows.

A (nontrivial) bridge-class a is said to lie within a particular zone if it contains a representative curve that lies entirely within

that zone (ignoring endpoints). Every (nontrivial) bridge-class lies within a unique zone.

Example: In Fig. 3c, classes a_1 , a_2 , and f lie within the resonance zone, and u_0, u_1, u_2, \dots lie within the external zone.

The homotopy class of an interval $W^U[\mathbf{p}, \mathbf{q}]$ can be expressed as a product of bridge-classes in a unique canonical form, called the *concise product*.

Definition 5 (concise product). A product of n (nontrivial) bridge-classes $a_1 \dots a_n$ is said to be concise if no two adjacent factors belong to the same zone.

The advantage of the concise product is that it allows one to determine topologically forced intersections. If $a_1 \dots a_n$ is the concise product of $[W^U[\mathbf{p}, \mathbf{q}]]$, then there is a topologically forced intersection of $W^U[\mathbf{p}, \mathbf{q}]$ with T^S between each pair of factors $a_i a_{i+1}$. This idea is further clarified by Lemma 2 in Sec. 3. Note this is only a minimal set of intersections, and there may, in fact, be more (unforced) intersections between $W^U[\mathbf{p}, \mathbf{q}]$ and T^S .

2.4. Dynamics of bridge-classes

The map M on phase space induces a new map (also denoted M) on homotopy classes, according to $M([A]) = [M(A)]$.

This new map satisfies the homomorphism properties $M(ab) = M(a)M(b)$ and $M(a^{-1}) = M(a)^{-1}$ for any classes a and b .

Example: We seek the first iterates of the bridge-classes $a_1, a_2, f, u_0, u_1, \dots$ shown in Fig. 3c. Fig. 3d and Fig. 3e show $M(a_1)$ and $M(a_2)$, from which we determine

$$M(a_1) = f^{-1}u_0a_2u_0^{-1}f, \quad (1)$$

$$M(a_2) = f^{-1}u_0^{-1}f. \quad (2)$$

Using $f = a_2a_1$ and the homomorphism properties of M , we also have

$$\begin{aligned} M(f) &= M(a_2a_1) = M(a_2)M(a_1) \\ &= (f^{-1}u_0^{-1}f)(f^{-1}u_0a_2u_0^{-1}f) = a_1^{-1}u_0^{-1}f. \end{aligned} \quad (3)$$

Finally, we see

$$M(u_n) = u_{n+1}. \quad (4)$$

Of particular importance are the iterates of each bridge-class expressed in concise form, as is the case for Eqs. (1) – (4). We call this the concise bridge dynamics. The concise bridge dynamics is important because the forward iterate $M(b)$ of a concise product $b = a_1\dots a_n$ may be obtained in concise form by simply replacing a_i with the concise representation of $M(a_i)$, for every i . Thus, we can map a concise product forward an arbitrary number of times into a new concise product by simply using the concise bridge dynamics as a set of substitution rules at each iterate.

The concise dynamics allow us to re-interpret each bridge class b as a *symbol* in symbolic dynamics. (Note that we do not consider b^{-1} to be a separate symbol.) A convenient way to visualize such dynamics is with a transition graph, in which there is a vertex for each symbol and in which a (directed) edge connects vertex a to vertex b if b (or b^{-1}) appears in $M(a)$. The edge is weighted by the number of appearances of either b or b^{-1} in $M(a)$. Figure 4 shows the transition graph for Eqs. (1) – (4). The transition graph can be represented by a transition matrix T , for which T_{ij} equals the number of copies of symbol i which occur in the iterate of symbol j , i.e. the weight of the edge connecting j to i .

All bridge-classes can be classified as either active or inert.

Definition 6 (inert and active bridge-classes). A bridge-class u is said to be inert if $M^n(u)$ is a bridge-class for all $n \geq 0$. A bridge-class is said to be active if it is not inert.

From this definition, we see that the inert bridge-classes form sequences $u_n, n \geq 0$, where $M(u_n) = u_{n+1}$. We call the first class u_0 the *primary* class of the sequence.

Example: The external bridge-class u_0 surrounding hole 3 in Fig. 3c is the primary inert class for the sequence of inert classes u_0, u_1, u_2, \dots (not shown), which surround holes 4, 5, The classes a_1, a_2 , and f are active.

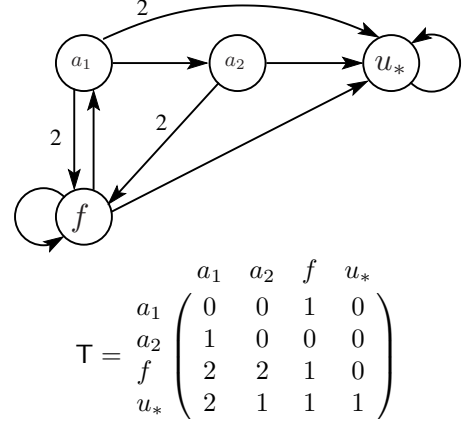


Figure 4: The transition graph and matrix for Eqs. (1) – (4). The symbol u_* represents all classes u_k . The edges connecting a_1 to f , a_1 to u_* , and a_2 to f each have weight 2. All other edges have weight 1.

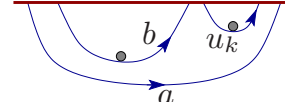


Figure 5: (Color online) The active classes a and b differ only by the inert class u_k , satisfying $a = bu_k$. Shaded circles denote holes.

Suppose two active bridge-classes a and b differ by an inert class u_k , e.g. $a = bu_k$ (Fig. 5). Then the forward iterates of a and b generate exactly the same forced intersections. In this sense, a and b are functionally equivalent, and so we symbolically identify a and b , i.e. we use the same symbol for both. Once we identify all such active classes, there are only a *finite* number of active bridge-classes.

Finally, we shall construct partition elements only for symbols in the *chaotic component* of the symbolic dynamics, defined as follows. First, define $a \sim b$ for two symbols a and b if b lies within the concise string $M^k(a)$ for some $k \geq 0$ and a lies within the concise string $M^{k'}(b)$ for some $k' \geq 0$. Equivalently, $a \sim b$ if there is a path in the transition graph connecting a to b and another path connecting b to a . The relation \sim partitions the set of symbols into equivalence classes, each of which is a strongly connected component of the transition graph. The dynamics can be restricted to each such component, and the topological entropy defined on it, using the restricted transition matrix. Some components may have zero topological entropy. For example every inert symbol forms a class unto itself with zero entropy. We shall, however, only be interested in those components with nonzero topological entropy. We refer to these as the *chaotic components* of the symbolic dynamics and the symbols in the chaotic components as the *chaotic symbols*. The chaotic components include only active symbols, though not every active symbol is necessarily in a chaotic component.

2.5. Algorithm to generate the concise dynamics of bridge-classes

To summarize, the algorithm below generates the set of bridge-classes \mathcal{B} and the concise product for $M(b)$, for each $b \in \mathcal{B}$. (See also [40].)

1. Beginning with a trellis T that satisfies the conditions in Sec. 2.1, identify the zone boundaries $T^S \cup \hat{T}^U$ and the corresponding zones.
2. Identify all pseudoneighbor pairs within the trellis. Punch a hole adjacent to one point in each pair of pseudoneighbors (Sec. 2.2), and identify the topological location of all forward and backward iterates of each hole. (Formally, holes should also be punched adjacent to each point $\mathbf{p} \in N$ and the preimages $M^n(\mathbf{p})$, $n < 0$.)
3. Identify all bridge-classes of bridges formed from segments of T^U , and note which zone each lies within (Sec. 2.3). Denote this set of bridge-classes by \mathcal{B} . (For simplicity, we need only include a bridge-class b or its inverse b^{-1} .)
4. For each primary inert bridge-class u_0 in \mathcal{B} , add the resulting infinite sequence of inert bridge-classes u_i , $i \geq 0$, into \mathcal{B} . Furthermore, use the same symbol for two bridge-classes a and au_i , where a is active, u_i is inert, and a and u_i are in the same zone. (Sec. 2.4.)
5. Express the forward iterate $M(b)$ of each active bridge-class $b \in \mathcal{B}$ as a product of bridge-classes. Whenever possible, take advantage of the group homomorphism property $M(ab) = M(a)M(b)$, for bridge-classes a , b , and ab (Sec. 2.4.)
6. For each $b \in \mathcal{B}$, express each forward iterate $M(b)$ in concise form (Sec. 2.3). If in constructing the concise form, a new bridge-class c is identified, add c into \mathcal{B} (noting which zone it lies within) and repeat from Step 4.

This algorithm is guaranteed to stop. After its completion, the chaotic components of the transition graph can be identified, as discussed in Sec. 2.4. It is for these chaotic symbols that we shall construct partition elements.

3. Distorted bridges

The concept of a bridge, as defined above, proves to be too restrictive for the construction of partition elements, requiring us to introduce a more flexible concept. As discussed in Sec. 2.5, the infinitely long unstable manifold W^U of the tangle is tightly constrained by the initial finite-length intervals T^U of the trellis. However, though the subsequent development of W^U beyond T^U is required to have a minimum set of topologically forced intersections with T^S , it typically contains additional intersections that are not topologically forced. This leads us to the concept of a distorted bridge.

Definition 7 (distorted bridge, D-bridge). *An unstable interval B is said to be a distorted bridge, or D-bridge for short, if B has only removable intersections, that is, if B can be homotopically distorted into a non-self-intersecting curve that only intersects T^S at the endpoints of B .*

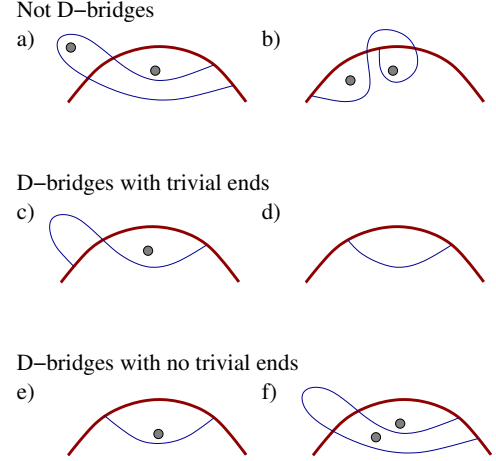


Figure 6: (Color online) Examples illustrating the concepts of D-bridges and trivial ends.

Examples (a) and (b) in Fig. 6 are clearly not D-bridges, but the remaining examples are. Note that all bridges are D-bridges, but not vice versa. Note also that the homotopy class of a D-bridge is, by Definition 4, a bridge class.

We shall primarily be interested in D-bridges that are topologically robust, as defined below. First, we introduce a few preliminary terms. An interval of W^U is said to be *degenerate* if it is a single point. An interval of W^U is said to be *trivial* if it is homotopically contractible to a point. A trivial interval B is said to be *even* or *odd* if it has an even or odd number of topologically transverse intersections with T^S . Thus, if the unstable manifold is continuously distorted so as to contract an odd trivial subinterval to a point, the resulting distorted curve maintains a transverse intersection with T^S at this point. On the other hand, if an even trivial subinterval is contracted to a point, that point may be shifted off of T^S , thereby removing all intersections from the original even subinterval. This is a simple consequence of the fact that intersection points annihilate one another in pairs of opposite orientation.

Definition 8 (trivial ends). *A trivial end of an unstable interval $B = W^U[\mathbf{p}, \mathbf{q}]$ is a (nondegenerate) trivial subinterval of B sharing a common endpoint with B .*

An interval $B = W^U[\mathbf{p}, \mathbf{q}]$ thus has no trivial ends if B contains no initial or final interval that is trivial, i.e. there are no (nondegenerate) intervals $W^U[\mathbf{p}, \mathbf{r}]$ or $W^U[\mathbf{r}, \mathbf{q}]$, with $\mathbf{r} \in W^U(\mathbf{p}, \mathbf{q})$, that are trivial. Examples (c) and (d) in Fig. 6 have trivial ends, whereas (e) and (f) do not. Also, a trivial interval, e.g. Fig. 6d, has a trivial end consisting of the entire interval. Note that any interval with trivial ends can be shortened into an interval with no trivial ends by simply trimming away the trivial ends. The trimmed interval clearly has the same homotopy class as the original. Henceforth, we focus on D-bridges without trivial ends.

A D-bridge $B = W^U[\mathbf{p}, \mathbf{q}]$ is said to be *robust* if, roughly speaking, it is topologically forced by the trellis T . This property can be characterized by examining the unstable intervals

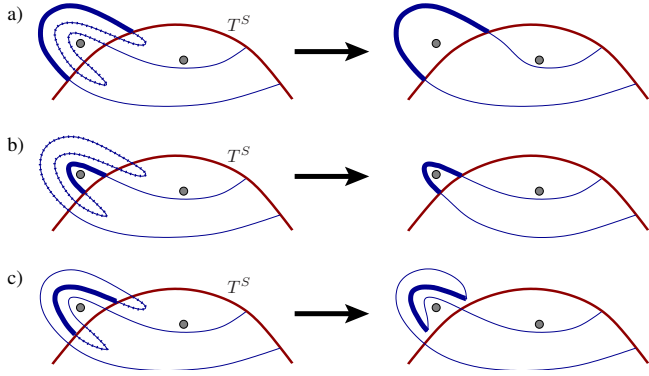


Figure 7: (Color online) The unstable manifold forms a switchback that illustrates the robustness property. The three bridges shown in thickest bold on the left sides of (a), (b), and (c) all have the same homotopy class (ignoring direction). However, the bold bridges in (a) and (b) are robust, whereas the bold bridge in (c) is not. The bridge in (a) has a trivial adjacent interval, shown as the hashed curve, that has an odd number of intersections, thereby satisfying the definition of robust. (Its other trivial adjacent interval is degenerate.) This hashed curve can be contracted to form the curve on the right. The same story applies in (b). In example (c), however, the two adjacent trivial intervals on either side of the bold bridge are even. When these intervals are contracted, the endpoints of the original bridge can themselves be removed from T^S . Thus, even though the bold interval in (c) is a bridge, it is not robust.

adjacent to the interval B in question. Consider the longest trivial interval $W^U[\mathbf{q}, \mathbf{r}]$ on one side of B and the longest trivial interval $W^U[\mathbf{s}, \mathbf{p}]$ on the other. We call these the *adjacent* trivial intervals of B . (Note that these intervals may be degenerate.) As noted previously, if an adjacent trivial interval is odd, it can be contracted to a point, leaving a single transverse intersection at the endpoint of B (Fig. 7a and Fig. 7b). If, however, the adjacent trivial interval is even, no transverse intersection is left, and the endpoint of B may be pulled off T^S (Fig. 7c). This removal of an endpoint of B from T^S means that B is not topologically robust. We thus define robust as follows.

Definition 9 (robust). *An interval is said to be robust if it has no trivial ends and if its adjacent trivial intervals are both odd.*

We introduce the abbreviation RoD-bridges for robust distorted bridges. RoD-bridges have several useful properties, summarized below. (Proofs are left to the interested reader.)

Lemma 1. *Two distinct RoD-bridges can only intersect at a common endpoint, i.e. they can not intersect along a common nondegenerate interval.*

Furthermore, we may decompose an unstable interval into a concatenation of RoD-bridges and trivial intervals.

Lemma 2 (RoD-bridge decomposition). *Denote the homotopy class of a robust unstable interval C by the concise product $[C] = a_1 \dots a_n$. Then C can be decomposed into a sequence of concatenated curves $A_1, e_1, A_2, e_2, \dots, e_{n-1}, A_n$, where A_i is a RoD-bridge with $[A_i] = a_i$ and where all the intermediate intervals e_i are trivial and odd (and possibly degenerate.) Thus, C intersects T^S at least $n - 1$ times (not including its endpoints). Note that the decomposition into A_i 's need not be unique.*

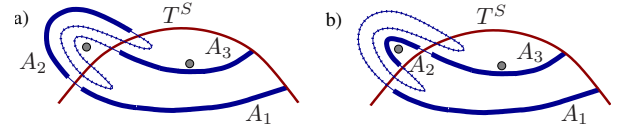


Figure 8: (Color online) Figures (a) and (b) show two RoD-bridge decompositions of the same interval. In each figure, the thickest bold curves indicate the three RoD-bridges in the decomposition, and the hashed curves are trivial intervals e_i . The first and last bridges A_1 and A_3 are the same for each decomposition. The middle bridge A_2 , however, differs between (a) and (b).

The nonuniqueness of this decomposition is illustrated in Fig. 8. The following refinement of Lemma 2 will allow us to define itineraries for RoD-bridges in Sec. 6.

Lemma 3 (RoD-bridge decomposition under forward iteration).

Let B be a RoD-bridge of class $b = [B]$ and $M(b) = a_1 \dots a_n$ the concise iterate of b .

(i) The iterate $M(B)$ of B is the concatenation of a sequence of RoD-bridges A_1, \dots, A_n , with $[A_i] = a_i$, such that the intervals between the A_i 's are trivial and odd. This decomposition is not necessarily unique.

(ii) For any RoD-bridge A contained within $M(B)$, there exists such a decomposition A_1, \dots, A_n of $M(B)$ for which $A = A_i$ for some i .

(iii) Though the decomposition specified in (ii) is not generally unique for a given A , the position of $A = A_i$ within such a decomposition (i.e. the value of i) is unique.

Figure 8 provides a helpful illustration of this lemma. Presuming the entire unstable interval in Fig. 8 to be the iterate $M(B)$ of some RoD-bridge B , statement (ii) is illustrated by the fact that each of the four RoD-bridges is part of some RoD-bridge decomposition, though there is no decomposition that contains all four simultaneously. Statement (iii) is illustrated by the fact that even though intervals A_1 and A_3 both appear in two different decompositions, their positions within those decompositions (i.e. first and third) are the same.

4. Orderings of RoD-bridges

As discussed in Sec. 2.3, a RoD-bridge is endowed with both a dynamical direction and, when viewed as a representative of a homotopy class, a homotopy direction. We focus here on the homotopy directions. For each homotopy class, it is convenient to select a reference orientation. That is, for any (nontrivial) bridge-classes b and b^{-1} , we choose either b or b^{-1} (for simplicity, say b) to define the *reference orientation* or *reference direction*.⁴ Recall that, in the figures, we denote the reference direction by barbed arrows.

Consider now two RoD-bridges B and B' whose initial endpoints (with respect to the *reference* orientation) lie on the same branch of T^S and which initially lie on the same side of T^S .

⁴A RoD-bridge with trivial class does not have a well defined reference direction.

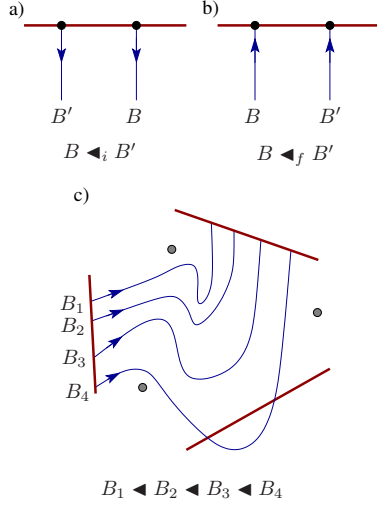


Figure 9: (Color online) An illustration of the conventions defining the orderings \triangleleft_i , \triangleleft_f , and \triangleleft .

Then we write $B \triangleleft_i B'$ if the initial point of B lies to the left of the initial point of B' , where left and right are defined while facing in the reference direction of B and B' , i.e. in the direction of the (barbed) arrows in Fig. 9a. We similarly define \triangleleft_f for final endpoints (Fig. 9b). These two relations, \triangleleft_i and \triangleleft_f , are (partial) orderings on the RoD-bridges.⁵

In general, $B \triangleleft_i B'$ need not imply $B \triangleleft_f B'$. However, if $[B] = [B']^{\pm 1}$, then: (i) B and B' are necessarily ordered by both \triangleleft_i and \triangleleft_f ; and (ii) these orderings agree, i.e. $B \triangleleft_i B'$ is equivalent to $B \triangleleft_f B'$. In this case, we simply write $B \triangleleft B'$. Thus, \triangleleft forms an order on all RoD-bridges within a bridge-class (Fig. 9c).

Two RoD-bridges B and B' satisfying $[B] \neq [B']^{\pm 1}$ may or may not be ordered by \triangleleft_i or \triangleleft_f . However, if they are ordered by \triangleleft_i or \triangleleft_f , this ordering is a function only of their bridge-classes, e.g. if $B \triangleleft_i B'$, then $A \triangleleft_i A'$ for any A and A' satisfying $[A] = [B]^{\pm 1}$ and $[A'] = [B']^{\pm 1}$. Hence, the \triangleleft_i and \triangleleft_f orderings are inherited by the bridge-classes. Specifically, for two bridge-classes b and b' , with $b' \neq b$, we define $b \triangleleft_i b'$ if $B \triangleleft_i B'$ for some B and B' where $b = [B]$ and $b' = [B']$ and where b and b' define the reference directions for B and B' . Note that the order of bridge-classes depends on their orientations, i.e. b versus b^{-1} ; reversing the directions of two bridge-classes reverses their ordering, i.e. $a \triangleleft_i a'$ implies $(a')^{-1} \triangleleft_i a^{-1}$.

Example: In Fig. 3c, the classes are ordered by

$$f^{-1} \triangleleft_f a_2^{-1} \triangleleft_f a_2 \triangleleft_f a_1^{-1} \triangleleft_f a_1 \triangleleft_f f, \quad (5)$$

$$f^{-1} \triangleleft_i a_1^{-1} \triangleleft_i a_1 \triangleleft_i a_2^{-1} \triangleleft_i a_2 \triangleleft_i f. \quad (6)$$

5. Definition of partition rectangles

5.1. Basic construction

For each chaotic symbol b , we construct a topological rectangle R_b with two stable sides and two unstable sides. We first

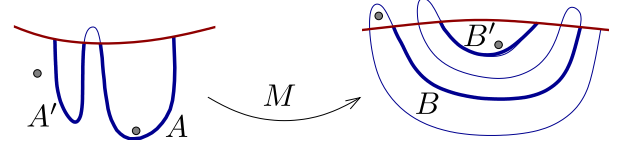


Figure 10: (Color online) On the right, B and B' (in thickest bold) are two RoD-bridges forming a switchback similar to that in Fig. 7. Their preimages $M^{-1}(B)$ and $M^{-1}(B')$ lie respectively in the bridges A and A' (in thickest bold) on the left. The bridge A is a RoD-bridge, but A' , being trivial, is not. Furthermore, there is no longer interval containing A' that is a RoD-bridge. Thus, $M^{-1}(B')$ does not lie within a RoD-bridge.

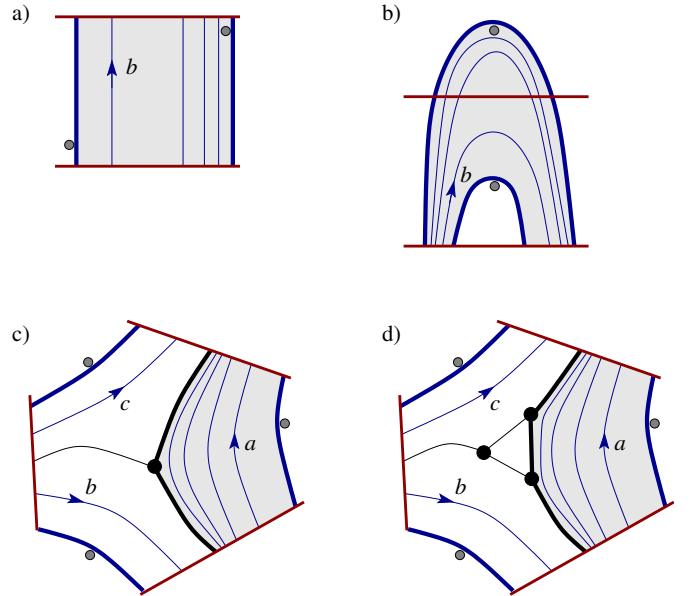


Figure 11: (Color online) Four examples of partition rectangles. In each, the rectangle is shaded and the unstable boundaries are in thickest bold.

⁵We typically omit the modifier “partial”.

restrict our attention to those RoD-bridges B such that an arbitrary preimage $M^{-n}(B)$ lies within some RoD-bridge A , for any $n > 0$. We shall expand on this concept when we discuss itineraries in Sec. 6, but for now we simply observe two facts. First, a RoD-bridge B need not have a preimage $M^{-1}(B)$ that lies within a RoD-bridge, as shown in Fig. 10. Second, Lemma 3 guarantees that there are an infinite number of RoD-bridges of a given chaotic symbol b that do have preimages $M^{-n}(B)$ lying within a RoD-bridge. Thus, for the remainder of this paper, we shall only consider those RoD-bridges having this preimage property, and cases like B' in Fig. 10 shall be ignored. With this understanding, the two unstable sides of the partition rectangle R_b are defined using the \blacktriangleleft ordering. In particular, one side is the supremum of all RoD-bridges of class b with respect to the \blacktriangleleft order, i.e. it is the upper limit of all RoD-bridges (satisfying the preimage property) with respect to this order. The other unstable side of the rectangle is the infimum of the \blacktriangleleft order. Collectively, we call the supremum and infimum the *boundary intervals* of class b .

Figure 11a illustrates an example of the boundary intervals, shown in bold, for a class b . The leftmost vertical line is the infimum interval. Immediately to its left is a hole, implying that there can be no unstable interval of class b farther to the left. The left boundary interval is itself a bridge of class b . The rightmost line is the supremum of b . This interval is also a bridge, but it is not in class b , since there is a hole immediately to its left. However, there is a sequence of bridges of class b converging upon it, as shown schematically in the figure. The point here is that the boundary intervals of a class b may or may not themselves be of class b .

Figure 11b illustrates an example in which the lower boundary interval, in bold, is again a bridge of class b , and the upper boundary interval, also in bold, is not of class b . Furthermore, the upper boundary is not a bridge or even a RoD-bridge, due to the hole immediately below it. Thus, we see that a boundary interval need not be a RoD-bridge.

Figure 11c illustrates an example showing three different bridge-classes, which surround a central unstable fixed point. This point is not an anchor and its three unstable branches are not branches of the trellis. Nevertheless, its branches form boundary intervals for the three classes. Focusing on class a , its right boundary is a bridge with class a . However, its left boundary consists of the two bold intervals connected to the central fixed point. Thus, we see that a boundary interval need not be an unstable interval of the tangle W^U . An unstable point with three branches is not structurally stable, and under a small perturbation, it bifurcates into a structure like that shown in Fig. 11d. Here, the vertices of the central triangle are periodic points, and the edges connecting them are very nearly separatrices.

In summary, though the unstable boundary intervals of a class b are the limits of RoD-bridges of class b , the intervals themselves need not have class b and need not be bridges, RoD-bridges, or even intervals of W^U .

Finally, the two *stable* boundaries of a partition rectangle are simply those stable intervals of T^S connecting the four endpoints of the unstable intervals.

5.2. Refined symbols

Suppose the forward iterate of a class a contains two or more copies of a class d (or its inverse), e.g. $M(a) = \dots d \dots d^{-1} \dots$. Such multiplicity creates obvious ambiguities in the symbolic itineraries. To resolve such ambiguities, we attach a unique index to each copy of d in the following geometrically meaningful way.

The rectangles in Fig. 12a illustrate the equation $M(a) = \dots d \dots d^{-1} \dots$. Here M folds the rectangle R_a into a horseshoe that intersects R_d twice, forming two smaller rectangles $R_d^{(i)}$ and $R_d^{(ii)}$. Note that we use the innermost fold (shown in bold) of the boundary of $M(R_a)$ to define the subrectangles. The new rectangle labels suggest the refined equation $M(a) = \dots d^{(i)} \dots d^{(ii)-1} \dots$. Despite this refinement a bridge lying within either $R_d^{(i)}$ or $R_d^{(ii)}$ still has homotopy class $d^{\pm 1}$.

Figure 12b illustrates a more complex example in which two symbols a and b each map twice to d . We again refine R_d into two smaller rectangles. We again use the innermost of the four folded boundary curves (in bold) to define the subrectangles. Finally, Fig. 12c illustrates even greater complexity, in which four rectangles map across R_d . In this case, there are two innermost folds (in bold), which define three subrectangles.

In general, innermost folds are constructed as follows. First, we define a fold as a pair of RoD-bridges D and D' such that both lie within $M(A)$ for some RoD-bridge A and both have the same homotopy class $d = [D]^{\pm} = [D']^{\pm}$, ignoring orientation. Considering all such folds for a given d (and for all possible A 's), we say that a pair D and D' forms an *innermost fold* if there is no other fold lying between them (as defined by the ordering of their endpoints along T^S)⁶. These innermost folds are then the cuts used to define the subrectangles $R_d^{(k)}$.

Once we have defined the subrectangles $R_d^{(k)}$, we can decorate each appearance of d in the concise dynamical equations with a superscript “ (k) ” to distinguish which subrectangle it lies within. We refer to $d^{(k)}$ as a *refined* symbol. For the remainder of this paper, we assume that all symbols have been refined, and the term symbol shall thus implicitly mean a refined symbol. With this refinement, a given chaotic symbol clearly never appears twice in the concise iterate of any one symbol.

Example: As previously determined, the concise dynamics for the active classes in Fig. 3 is

$$M(a_1) = f^{-1} u_0 a_2 u_0^{-1} f, \quad (7)$$

$$M(a_2) = f^{-1} u_0^{-1} f, \quad (8)$$

$$M(f) = a_1^{-1} u_0^{-1} f. \quad (9)$$

The class f is repeated in the iterates of both a_1 and a_2 . To avoid this repetition, we consider Fig. 13a, which illustrates the topology of $M(a_1)$ and $M(a_2)$. Fig. 13b illustrates the same topology, but distorted to straighten the intervals of class f . These intervals are labelled I, II, III, and IV. From this figure,

⁶An innermost fold may also arise as the lower limit of nested folds, consisting thus of limits of RoD-bridges, as discussed in Sec. 5.1.

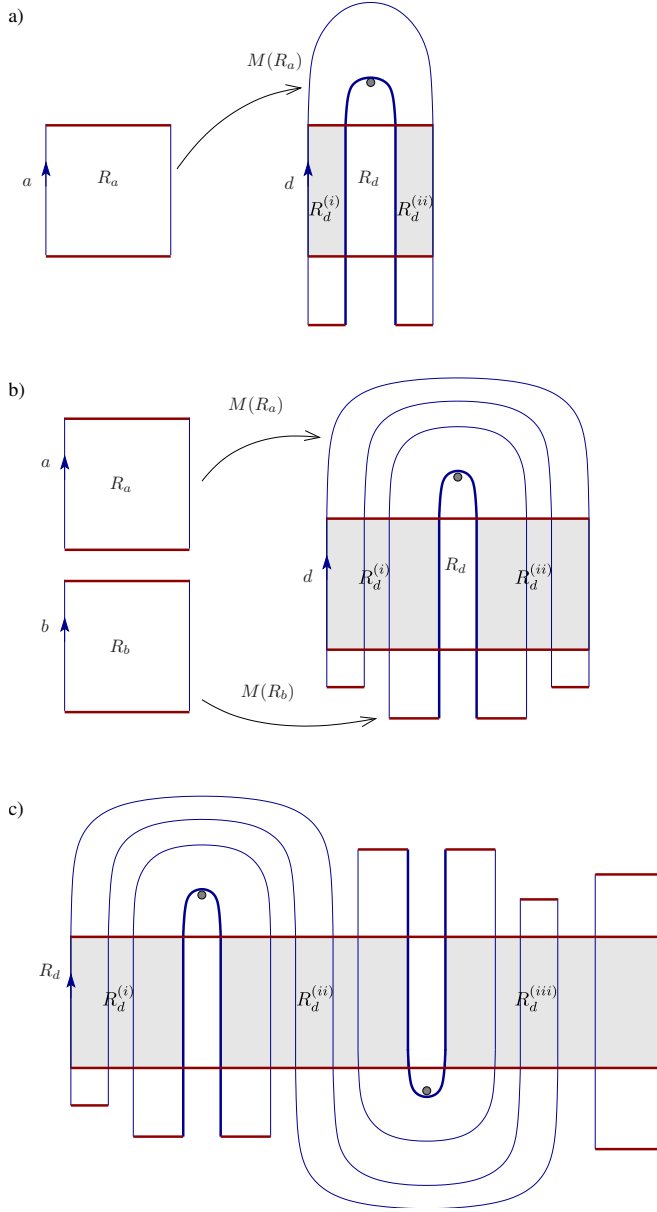


Figure 12: (Color online) Illustrations of subdividing a partition rectangle R_d to enforce uniqueness in forward iteration.

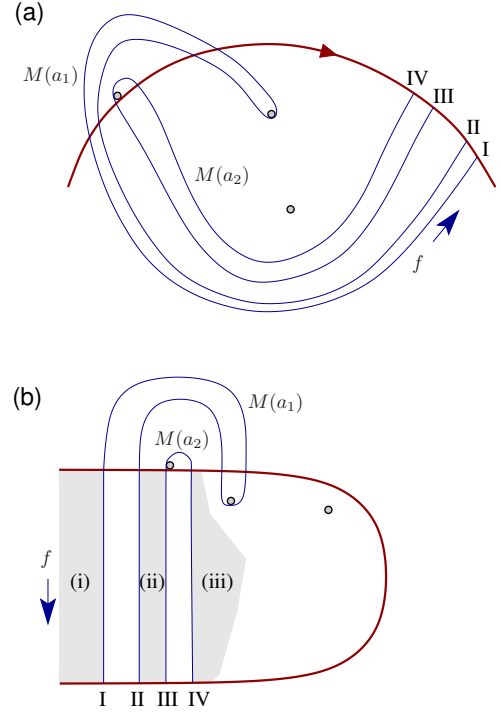


Figure 13: (Color online) Figure (a) is a qualitative illustration of $M(a_1)$ and $M(a_2)$ shown in Figs. 3d and 3e. Figure (b) distorts (a) so that the f bridges are straightened out.

it is obvious that the pair I and II and the pair III and IV form inner folds, which give us three subrectangles, labelled (i), (ii), and (iii). The concise dynamics for a_1 and a_2 is then refined by the top equations in Fig. 14. Furthermore, though we now distinguish the refined symbols $f^{(i)}$, $f^{(ii)}$, and $f^{(iii)}$, their iterates are all identical, as shown at the top of Fig. 14, a fact that is true in general for refined symbols.

Note that each RoD-bridge not only has a homotopy class, but it also can be assigned a well defined (refined) symbol. A RoD-bridge B is assigned the (refined) symbol b if B can be homotopically distorted into a curve lying entirely within R_b without moving the endpoints of B .

Note that the orders defined in Sec. 4 extend naturally to the refined symbols, and hence the basic construction of partition rectangles in Sec. 5.1 applies to the refined dynamics. That is, the unstable boundary intervals of R_b , where b is a (refined) symbol, are the infimum and supremum of all RoD-bridges with symbol b .

An important point of this construction is that the partition rectangles are compatible with the original homotopic lobe dynamics in the following sense.

Theorem 1. *For every bi-infinite sequence $\dots s_{-1}s_0s_1\dots$ of chaotic symbols that is allowed by the homotopic lobe dynamics, there is at least one orbit $x_k = M^k(x_0)$ with $x_k \in R_{s_k}$ for all k .*⁷

⁷This theorem follows directly from Lemma 3.

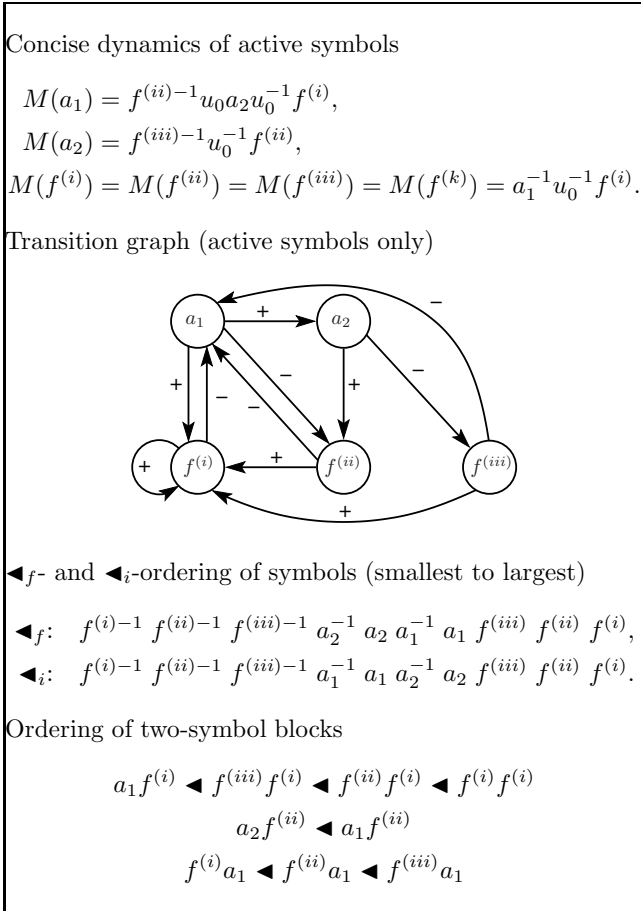


Figure 14: Summary of symbolic dynamics for the example in Fig. 3 using the refinement of f in Fig. 13.

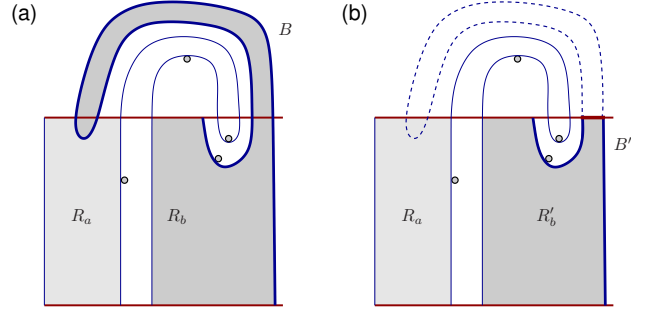


Figure 15: (Color online) (a) An example of rectangles intersecting with nonzero area. (b) The intersection between R_a and R_b shown in part (a) can be removed by trimming R_b to R'_b .

In general, the partition is not a generating partition, which would yield a topological equivalence between the symbolic dynamics and the map dynamics. However, the symbolic dynamics can be made arbitrarily accurate, as discussed in Secs. 9 and 10.

Finally, we note that the partition rectangles defined above can intersect. Such intersections might only occur at the rectangle boundaries, as for R_a , R_b , and R_c in Figs. 11c and 11d. Such boundary intersections commonly occur when partitioning, even for the simple case of unimodal maps. However, the intersections of partition rectangles defined above can potentially be more significant, as illustrated in Fig. 15a, where the unstable boundary B (in bold) of R_b is a RoD-bridge that intersects the interior of R_a . Since this intersection is not topologically forced, however, B can be distorted into the curve B' in Fig. 15b (in bold) by removing the dashed trivial interval. This creates a trimmed partition element R'_b . This trimming can be carried out in general, and in such a manner that the resulting partition elements only intersect at their boundaries and that they still satisfy Theorem 1. For the remainder of this paper, we utilize the partition rectangles as originally formulated above, recognizing that these could be trimmed if so desired.

6. RoD-Bridge itineraries

We demonstrate here how RoD-bridges can be labelled with symbolic itineraries. In Secs. 7 and 8 we shall explain how to find such itineraries for the boundary intervals of a partition rectangle.

6.1. Initial construction

We consider a RoD-bridge B_0 , which, as we have been assuming, satisfies the preimage property of Sec. 5.1, i.e. $M^{-n}(B_0)$ lies within a RoD-bridge for all $n > 0$. There is thus a unique infinite sequence of RoD-bridges $\dots, B_{-2}, B_{-1}, B_0$, such that $B_{i+1} \subset M(B_i)$. We call the RoD-bridges B_i the *ancestors* of B_0 . Every ancestry sequence $\dots, B_{-2}, B_{-1}, B_0$ has an infinite periodic beginning. To see this, consider an *anchor* bridge $A_0 = T^U[\mathbf{z}, \mathbf{p}]$, $\mathbf{z} \in P$, $\mathbf{p} \in N$. Each ancestor A_i of A_0 must have one periodic endpoint in P , and hence must itself be an anchor bridge. The ancestry sequence $\dots, A_{-2}, A_{-1}, A_0$

must therefore be periodic with period equal to the branch period. Since the anchor bridges generate all of W^U , an arbitrary RoD-bridge B_0 must have some anchor bridge A_0 in its ancestry, and hence going back in time, the ancestry sequence $\dots, B_{-2}, B_{-1}, B_0$ must eventually be periodic, with form $\dots, A_{-2}, A_{-1}, A_0, \dots, B_{-2}, B_{-1}, B_0$. Thus, only a finite number of ancestors of B_0 is truly important.

Since each ancestor B_i has a symbol b_i , we can associate an infinite *itinerary* of symbols $\dots b_{-2}b_{-1}b_0$ to a RoD-bridge B_0 . (The symbols b_i are assumed to be refined according to the discussion in Sec. 5.2.) The symbol a_i of an anchor bridge A_i is called an *anchor symbol*, and the periodic ancestry sequence $\dots, A_{-2}, A_{-1}, A_0$ of an anchor bridge A_0 generates a periodic itinerary of anchor symbols $\dots a_{-2}a_{-1}a_0$. There are clearly a finite number of such *anchor itineraries*, one for each unstable branch of the trellis. Since the ancestry sequence of any RoD-bridge B_0 begins with anchor bridges, the itinerary of B_0 must begin with an anchor itinerary, i.e. $\dots a_{-2}a_{-1}a_0 \dots b_{-2}b_{-1}b_0$.

Consider now an allowable itinerary $b_{-n} \dots b_{-2}b_{-1}b_0$ of finite length and a RoD-bridge B_{-n} with symbol b_{-n} . Lemma 3, part (i), guarantees the existence of a sequence of RoD-bridges $B_{-n}, \dots, B_{-2}, B_{-1}, B_0$, with $B_{i+1} \subset M(B_i)$ and with b_i the symbol of B_i .

Consider now an allowable itinerary $\dots a_{-2}a_{-1}a_0 \dots b_{-2}b_{-1}b_0$ of infinite length and beginning with an anchor itinerary. Considering only the finite itinerary $a_0 \dots b_{-2}b_{-1}b_0$ and the (unique) anchor bridge A_0 with symbol a_0 , our preceding assertion shows that there is a sequence $A_0, \dots, B_{-2}, B_{-1}, B_0$ of RoD-bridges with itinerary $a_0 \dots b_{-2}b_{-1}b_0$. Hence, given an allowable itinerary $\dots a_{-2}a_{-1}a_0 \dots b_{-2}b_{-1}b_0$, beginning with an anchor itinerary, there exists a RoD-bridge B_0 with that itinerary. Note, however, that since the decomposition in Lemma 3 is not necessarily unique, B_0 need not be uniquely determined by its itinerary.

6.2. Itineraries with chaotic symbols only

Note that the symbols used in the itineraries above may or may not be chaotic, i.e. in the chaotic component of the dynamics. We show here how we can restrict our attention to itineraries consisting only of chaotic symbols.

Recalling Sec. 5.1, the unstable boundary intervals of a partition rectangle R_b are the supremum and infimum of all RoD-bridges with symbol b (and satisfying the preimage condition). As previously noted, these boundary intervals need not themselves be RoD-bridges with symbol b ; they are simply the limits of such RoD-bridges. We shall thus introduce the shorthand limRoD-bridge (“lim” for limit) for an interval B that is the limit of a sequence of RoD-bridges B_i , with $B_i \neq B$, converging on either the right (positive) side or left (negative) side of B , as defined by the dynamical orientation of B . A limRoD-bridge could have either a left-converging sequence, a right-converging sequence, or both. As already noted, a limRoD-bridge need not be a RoD-bridge (as in Fig. 11b, c, and d; see also Fig. 16.) Furthermore, a RoD-bridge need not be a limRoD-bridge (since $B_i \neq B$).

For a limRoD-bridge B with a right-converging sequence B_i , we define the homotopy class $[B]_+$ as the class $\lim_{i \rightarrow \infty} [B_i]$.

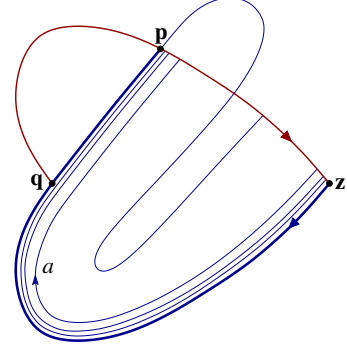


Figure 16: (Color online) The thickest bold interval $A = T^U[\mathbf{z}, \mathbf{p}]$ is a limRoD-bridge, with a sequence of three bridges shown converging upon it. These bridges have symbol a , which implies $[A]_+ = a$. Since one of the endpoints of A is an anchor $\mathbf{z} \in P$, A is an anchor limRoD-bridge and a is an anchor symbol. Note that the shorter interval $T^U[\mathbf{z}, \mathbf{q}]$ is an anchor bridge, but is not a limRoD-bridge; $T^U[\mathbf{q}, \mathbf{p}]$ is a bridge, but neither a limRoD-bridge nor an anchor bridge.

Equivalently, $[B]_+ = [B_{+\epsilon}]$, where $B_{+\epsilon}$ is a RoD-bridge that is an arbitrarily small perturbation of B to the right. An analogous definition holds for the class $[B]_-$. Furthermore, we shall assume for the remainder of the paper that all symbols $[B]_{\pm}$ are refined as in Sec. 5.2.

Analogous to prior definitions, an *anchor* limRoD-bridge is a limRoD-bridge $A = T^U[\mathbf{z}, \mathbf{p}]$, with $\mathbf{z} \in P$, $\mathbf{p} \in T^S \cap T^U$. Note that an anchor limRoD-bridge need not be an anchor RoD-bridge (see Fig. 16), and so we extend the term *anchor symbol* to include all symbols $[A]_{\pm}$ of anchor limRoD-bridges.

We now adapt the results in Sec. 6.1 to limRoD-bridges. As before we consider only those limRoD-bridges B satisfying the preimage condition, i.e. that the preimage of B lies within a limRoD-bridge. Thus, for a limRoD-bridge B_0 , we can construct a sequence of ancestors $\dots, B_{-2}, B_{-1}, B_0$, such that $B_{i+1} \subset M(B_i)$ and where each B_i is a limRoD-bridge. As before, such sequences begin with a periodic sequence of anchor limRoD-bridges $\dots, A_{-2}, A_{-1}, A_0$. Suppose $b_0 = [B_0]_+$, then the ancestry sequence of B_0 gives rise to an itinerary $\dots a_{-2}a_{-1}a_0 \dots b_{-2}b_{-1}b_0$ that begins with an anchor itinerary and where $b_i = [B_i]_+$; the analogous result holds for $b_0 = [B_0]_-$. Furthermore, it is possible for a limRoD-bridge to have two such itineraries, one constructed from $b_i = [B_i]_+$ and one from $b_i = [B_i]_-$. Finally, so long as b_0 is a chaotic symbol, the entire itinerary b_i consists of *chaotic* symbols.

To summarize, every limRoD-bridge B_0 for which $b_0 = [B_0]_{\pm}$ is chaotic has an itinerary $\dots a_{-2}a_{-1}a_0 \dots b_{-2}b_{-1}b_0$ consisting only of chaotic symbols $b_i = [B_i]_{\pm}$ and beginning with an anchor itinerary.

The converse is also true. For every allowable itinerary $\dots a_{-2}a_{-1}a_0 \dots b_{-2}b_{-1}b_0$ of chaotic symbols that begins with an anchor itinerary, there exists a limRoD-bridge B_0 with that itinerary. This follows from Lemma 3, adapted to limRoD-bridges.

7. Computing orderings from itineraries

In Sec. 4 we defined the two RoD-bridge orderings \blacktriangleleft_i and \blacktriangleleft_f , and in Sec. 6 we discussed how RoD-bridges could be labeled by symbolic itineraries. Here we demonstrate how the orderings of RoD-bridges can be determined by their itineraries alone.

Consider two itineraries $\dots s_{-1}s_0$ and $\dots s'_{-1}s'_0$. If these itineraries label unique RoD-bridges B and B' , then the \blacktriangleleft_i and \blacktriangleleft_f orderings can be determined from the itineraries alone. We thus adopt the notation $\dots s_{-1}s_0 \blacktriangleleft \dots s'_{-1}s'_0$ to mean $B \blacktriangleleft B'$, and similarly for \blacktriangleleft_i and \blacktriangleleft_f . If $s_0 \neq s'_0$, then the RoD-bridges B and B' have different symbols, and their orderings, if well defined, are determined by the symbols s_0 and s'_0 alone, as previously observed in Sec. 4. The ordering between different symbols is readily extracted from the geometry of the initial trellis. In the following, we thus assume that for any two symbols s_0 and s'_0 , with $s_0 \neq s'_0$, we know whether $s_0 \blacktriangleleft_i s'_0$ or $s'_0 \blacktriangleleft_i s_0$, and similarly for \blacktriangleleft_f .

We now concentrate on the case $s_0 = s'_0$, i.e. the case in which the RoD-bridges being compared have the same symbol. In this case the two orders \blacktriangleleft_i and \blacktriangleleft_f reduce to the single order \blacktriangleleft . We initially focus on only the last two symbols in the itineraries, $s_{-1}s_0$ and $s'_{-1}s_0$, and assume $s_{-1} \neq s'_{-1}$. We define the parity $\pi(s_{-1}s_0)$ of a two-symbol block by whether s_0 or s_0^{-1} appears in the iterate of s_{-1} , i.e.

$$\pi(s_{-1}s_0) = \begin{cases} +1 & \text{if } M(s_{-1}) = \dots s_0 \dots, \\ -1 & \text{if } M(s_{-1}) = \dots s_0^{-1} \dots \end{cases} \quad (10)$$

Thus, defining $\epsilon = \pi(s_{-1}s_0)$ and $\epsilon' = \pi(s'_{-1}s_0)$, we have

$$M(s_{-1}^\epsilon) = \dots s_0 \dots, \quad (11)$$

$$M(s'_{-1}^{\epsilon'}) = \dots s_0 \dots \quad (12)$$

We then introduce the following notation for the symbols immediately before and after s_0 in the iterate

$$M(s_{-1}^\epsilon) = \dots ab_1 \dots b_j s_0 c_1 \dots c_k d \dots, \quad (13)$$

$$M(s'_{-1}^{\epsilon'}) = \dots a' b_1 \dots b_j s_0 c_1 \dots c_k d' \dots, \quad (14)$$

where the blocks $b_1 \dots b_j$ and $c_1 \dots c_k$ are common to both iterates, and where $a \neq a'$ and $d \neq d'$. Thus, a and a' are the closest distinct symbols that precede s_0 , and d and d' are the closest distinct symbols that follow s_0 . Note that if all the symbols that precede s_0 were equal in $M(s_{-1}^\epsilon)$ and $M(s'_{-1}^{\epsilon'})$, then a and a' would fail to exist. Similarly, d and d' would fail to exist if all the symbols that follow s_0 were equal.

Assume a and a' exist, and consider the homotopy classes $ab_1 \dots b_j s_0$ and $a' b_1 \dots b_j s_0$ (Fig. 17). Since a and a' are distinct with final endpoints on the same stable branch, they are ordered by \blacktriangleleft_f . (In Fig. 17, $a \blacktriangleleft_f a'$.) The order of a and a' is then the same as that of $s_{-1}s_0$ and $s'_{-1}s_0$, i.e. $a \blacktriangleleft_f a' \Leftrightarrow s_{-1}s_0 \blacktriangleleft s'_{-1}s_0$.

Assume now that a and a' fail to exist. Then, since M preserves orientation, $s_{-1}s_0$ and $s'_{-1}s_0$ acquire the initial ordering of s_{-1}^ϵ and $s'_{-1}^{\epsilon'}$, i.e. $s_{-1}^\epsilon \blacktriangleleft_i s'_{-1}^{\epsilon'} \Leftrightarrow s_{-1}s_0 \blacktriangleleft s'_{-1}s_0$. In summary

$$s_{-1}s_0 \blacktriangleleft s'_{-1}s_0 \Leftrightarrow \begin{cases} a \blacktriangleleft_f a' & \text{if } a \text{ and } a' \text{ exist,} \\ s_{-1}^\epsilon \blacktriangleleft_i s'_{-1}^{\epsilon'} & \text{otherwise.} \end{cases} \quad (15)$$

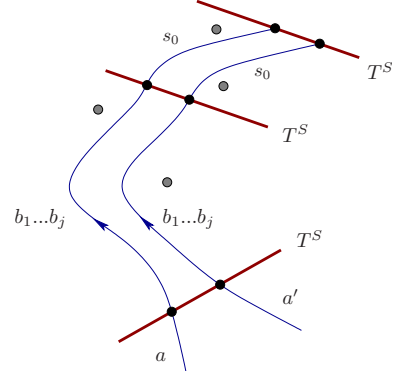


Figure 17: (Color online) An illustration of the notation in Eqs. (13) and (14).

This result can be neatly restated if we define a new notational use of \blacktriangleleft . For two symbol strings S and S' ,

$$\blacktriangleleft(S, S') = \begin{cases} +1 & \text{if } S \blacktriangleleft S', \\ -1 & \text{if } S \blacktriangleright S'. \end{cases} \quad (16)$$

Similar usage applies to $\blacktriangleleft_i(S, S')$ and $\blacktriangleleft_f(S, S')$. Then Eq. (15) is equivalent to

$$\blacktriangleleft(s_{-1}s_0, s'_{-1}s_0) = \begin{cases} \blacktriangleleft_f(a, a') & \text{if } a \text{ and } a' \text{ exist,} \\ \blacktriangleleft_i(s_{-1}^\epsilon, s'_{-1}^{\epsilon'}) & \text{otherwise.} \end{cases} \quad (17)$$

Similarly, we can express the criterion in terms of the d and d' classes in Eqs. (13) and (14) instead.

$$\blacktriangleleft(s_{-1}s_0, s'_{-1}s_0) = \begin{cases} \blacktriangleleft_i(d, d') & \text{if } d \text{ and } d' \text{ exist,} \\ \blacktriangleleft_f(s_{-1}^\epsilon, s'_{-1}^{\epsilon'}) & \text{otherwise.} \end{cases} \quad (18)$$

Example: In Fig. 3, there are five active symbols a_1 , a_2 , $f^{(i)}$, $f^{(ii)}$, and $f^{(iii)}$, accounting for the refinement of f in Fig. 13. Updating (5) and (6) for the refinement of f , the \blacktriangleleft_f - and \blacktriangleleft_i -orderings are recorded in Fig. 14. The top of Fig. 14 contains the concise dynamics, from which we extract the following two-symbol blocks $s_{-1}s_0$ and parities $\pi(s_{-1}s_0)$.

$$\begin{aligned} \pi = +1: & \quad a_1 a_2 \quad a_1 f^{(i)} \quad a_2 f^{(ii)} \quad f^{(k)} f^{(i)} \\ \pi = -1: & \quad a_1 f^{(ii)} \quad a_2 f^{(iii)} \quad f^{(k)} a_1 \end{aligned} \quad (19)$$

where $f^{(k)}$ can be either $f^{(i)}$, $f^{(ii)}$, or $f^{(iii)}$. These parities label the edges in the transition graph of Fig. 14. We next compute the \blacktriangleleft -order of all two-symbol blocks $s_{-1}s_0$ and $s'_{-1}s_0$. Starting with $a_1 f^{(i)}$ and $f^{(iii)} f^{(i)}$, we note

$$\begin{aligned} M(a_1) &= f^{(ii)-1} u_0 a_2 (u_0^{-1} f^{(i)}), \\ M(f^{(iii)}) &= a_1^{-1} (u_0^{-1} f^{(i)}). \end{aligned} \quad (20)$$

which should be compared to Eqs. (13) and (14), with $a = a_2$ and $a' = a_1^{-1}$. Since $a_2 \blacktriangleleft_f a_1^{-1}$ [see \blacktriangleleft_f -ordering in Fig. 14], Eq. (15) implies $a_1 f^{(i)} \blacktriangleleft f^{(iii)} f^{(i)}$. Continuing with $f^{(i)} f^{(i)}$ and $f^{(ii)} f^{(i)}$, since

$M(f^{(i)}) = M(f^{(ii)})$, a and a' in Eqs. (13) and (14) do not exist, so that we must use the second case in Eq. (15). Then, since $f^{(ii)} \triangleleft_i f^{(i)}$ [see \triangleleft_i -ordering in Fig. 14], we find $f^{(ii)} f^{(i)} \triangleleft f^{(i)} f^{(i)}$. In a similar manner, we can complete the orderings for all two-symbol blocks ending in $f^{(i)}$, as recorded at the bottom of Fig. 14.

Moving to itineraries ending in $f^{(ii)}$, we consider $a_1 f^{(ii)}$ and $a_2 f^{(ii)}$, for which

$$\begin{aligned} M(a_1^{-1}) &= f^{(i)-1} u_0 a_2^{-1} (u_0^{-1} f^{(ii)}), \\ M(a_2) &= f^{(iii)-1} (u_0^{-1} f^{(ii)}). \end{aligned} \quad (21)$$

Again applying Eq. (15), since $f^{(iii)-1} \triangleleft_f a_2^{-1}$, we have $a_2 f^{(ii)} \triangleleft a_1 f^{(ii)}$, as recorded in Fig. 14.

Finally, considering itineraries ending in a_1 , we have $f^{(i)} a_1$, $f^{(ii)} a_1$, and $f^{(iii)} a_1$. Using the fact that $M(f^{(i)-1}) = M(f^{(ii)-1}) = M(f^{(iii)-1}) = f^{(i)-1} u_0 a_1$ and that $f^{(i)-1} \triangleleft_i f^{(ii)-1} \triangleleft_i f^{(iii)-1}$, the second case of Eq. (15) implies $f^{(i)} a_1 \triangleleft f^{(ii)} a_1 \triangleleft f^{(iii)} a_1$, as recorded in Fig. 14.

Next consider two three-symbol blocks of the form $s_{-2} s_{-1} s_0$ and $s'_{-2} s_{-1} s_0$, where $s_{-2} \neq s'_{-2}$. Then $M(s_{-1})$ has the form

$$M(s_{-1}) = \dots s_0^\epsilon \dots, \quad (22)$$

with $\epsilon = \pi(s_{-1} s_0)$. If ϵ is positive, then the order of $s_{-2} s_{-1} s_0$ and $s'_{-2} s_{-1} s_0$ is simply the order of $s_{-2} s_{-1}$ and $s'_{-2} s_{-1}$, i.e. $\triangleleft(s_{-2} s_{-1} s_0, s'_{-2} s_{-1} s_0) = \triangleleft(s_{-2} s_{-1}, s'_{-2} s_{-1})$, otherwise the order is reversed, i.e. $\triangleleft(s_{-2} s_{-1} s_0, s'_{-2} s_{-1} s_0) = -\triangleleft(s_{-2} s_{-1}, s'_{-2} s_{-1})$. These two cases can be summarized as

$$\triangleleft(s_{-2} s_{-1} s_0, s'_{-2} s_{-1} s_0) = \triangleleft(s_{-2} s_{-1}, s'_{-2} s_{-1}) \pi(s_{-1} s_0). \quad (23)$$

For longer blocks, parity is defined by multiplying the parity for each transition, i.e. $\pi(s_{-n} \dots s_0) = \prod_{i=-n}^{-1} \pi(s_i s_{i+1})$. Equation (23) for three-symbol blocks now generalizes to arbitrary numbers of symbols

$$\begin{aligned} \triangleleft(\dots s_{-n} s_{-n+1} \dots s_{-1} s_0, \dots s'_{-n} s_{-n+1} \dots s_{-1} s_0) = \\ \triangleleft(s_{-n} s_{-n+1}, s'_{-n} s_{-n+1}) \pi(s_{-n+1} \dots s_0), \end{aligned} \quad (24)$$

where s_{-n} and s'_{-n} is the first pair of symbols, moving right to left, which are not equal. Equation (24) shows that the ordering of two itineraries reduces to the ordering of two-symbol blocks.

8. Constructing the boundary intervals

To find the two boundary intervals of a given chaotic symbol s , we first find their itineraries. These are the maximum and minimum itineraries, with respect to \triangleleft , having the form $\dots s_{-2} s_{-1} s$, where the s_i are chaotic symbols. (All symbols are assumed chaotic in this section.) The results of Sec. 7 make it straightforward to determine these two itineraries. Suppose we wish to determine the maximum itinerary $\dots s_{-2} s_{-1} s$. Then s_{-1} is simply that symbol which maximizes the two-symbol sequences $s' s$, i.e. $s' s \triangleleft s_{-1} s$, or equivalently \triangleleft

terminal symbol	maximum	minimum
a_1	$\overline{a_2 f^{(iii)} a_1}$	$\overline{f^{(i)} a_1}$
a_2	$\overline{f^{(iii)} a_1 a_2}$	$\overline{f^{(i)} a_1 a_2}$
$f^{(i)}$	$\overline{f^{(i)}}$	$\overline{f^{(i)} a_1 f^{(i)}}$
$f^{(ii)}$	$\overline{f^{(i)} a_1 f^{(ii)}}$	$\overline{f^{(i)} a_1 a_2 f^{(ii)}}$
$f^{(iii)}$	$\overline{f^{(i)} a_1 a_2 f^{(iii)}}$	$\overline{a_1 a_2 f^{(iii)}}$

Table 1: Extreme itineraries for symbolic dynamics in Fig. 14.

$(s' s, s_{-1} s) = 1$, for all allowed symbols $s' \neq s_{-1}$. Working backwards, if $\pi(s_{-1} s) = 1$, Eq. (23) implies that the next symbol s_{-2} is the symbol that maximizes two-symbol itineraries of the form $s' s_{-1}$. If $\pi(s_{-1} s) = -1$, however, s_{-2} is the symbol that minimizes such itineraries. Both cases are summarized by the requirement that s_{-2} satisfy $\triangleleft(s' s_{-1}, s_{-2} s_{-1}) = \pi(s_{-1} s)$ for all allowed symbols $s' \neq s_{-2}$. In this manner, we work recursively backwards, at each step choosing s_{-k} to satisfy $\triangleleft(s' s_{-k+1}, s_{-k} s_{-k+1}) = \pi(s_{-k+1} \dots s_{-1} s)$ for all allowed $s' \neq s_{-k}$, thereby generating the entire maximum itinerary. Thus, we only need to know the parity and ordering of all two-symbol blocks to find the maximum itinerary ending in s . The algorithm for the minimum itinerary is exactly the same, except at each step we choose s_{-k} according to $\triangleleft(s' s_{-k+1}, s_{-k} s_{-k+1}) = -\pi(s_{-k+1} \dots s_{-1} s)$ for all allowed $s' \neq s_{-k}$.

In principle, the extreme itineraries are infinitely long. However, since there are a finite number of chaotic symbols, an extreme itinerary $\dots s_{-2} s_{-1} s$ constructed recursively must eventually become periodic as one moves to the left, i.e. an extreme itinerary has the form $\overline{a_{-p+1} \dots a_{-1} a_0} s_{-n} \dots s_{-1} s$, beginning with the sequence $\overline{a_{-p+1} \dots a_{-1} a_0} = \dots (a_{-p+1} \dots a_{-1} a_0) (a_{-p+1} \dots a_{-1} a_0)$ of period p . (Here, an overbar denotes an infinite repetition.) If this periodic sequence is one of the anchor sequences discussed in Sec. 6, the corresponding unstable interval (which is a limRoD-bridge) lies within the unstable manifold of the tangle W^U . However, the periodic sequence need not be an anchor sequence, in which case the corresponding interval lies within the unstable manifold of a periodic point that is not in the original set of anchor points P , as illustrated previously in Fig. 11c and Fig. 11d.

Example: For the example in Fig. 3, we have previously computed the parity and ordering of all two-symbol itineraries (Fig. 14). We now work through a few examples to show how to compute maximum and minimum itineraries.

maximum itinerary ending in a_1 : We refer to the table below which shows each new symbol being

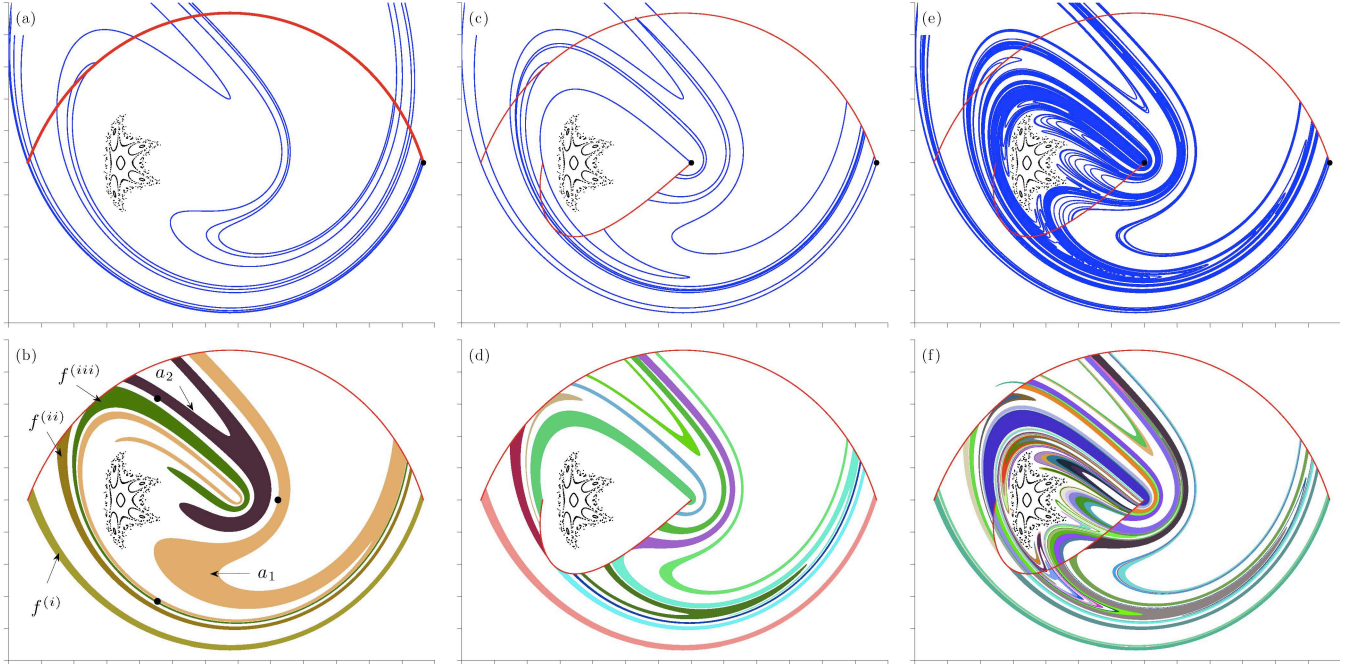


Figure 19: (Color online) The top row shows three trellises, all computed from the same map used in Fig. 3, with 19a being the same trellis as Fig. 3a and 19c being essentially the same as Fig. 20a. The lengths of the manifolds and the number of branches increases from a to c to e. The bottom row shows the partition corresponding to each trellis, with colors assigned randomly to each partition element. The partitions resolve the dynamics in the vicinity of the stable zone with increasing accuracy. The number of partition elements in b, d, and f are 5, 13, and 80, respectively.

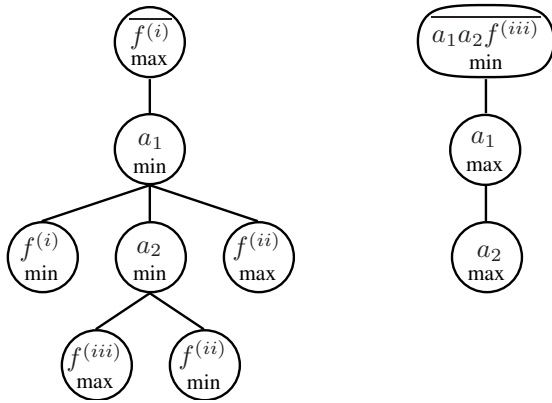


Figure 18: Extreme itinerary tree graphically organizing the itineraries in Table 1.

added.

Step	Constructed Itinerary	Total Parity π
1	$f^{(iii)} a_1$	
	-1	-1
2	$a_2 f^{(iii)} a_1$	
	-1 -1	+1
3	$a_1 a_2 f^{(iii)} a_1$	
	+1 -1 -1	+1

$$\text{final itinerary} = \overline{a_2 f^{(iii)} a_1}$$

Of all two-symbol itineraries ending in a_1 , $f^{(iii)} a_1$ is the greatest [See bottom of Fig. 14], so the top row of the table begins with $f^{(iii)} a_1$. Immediately below $f^{(iii)} a_1$, we place its parity $\pi(f^{(iii)} a_1) = -1$. The right hand column lists the total parity of the itinerary constructed thus far, initially just -1. Since this total parity is negative, the symbol added at step 2 is the one that makes the *smallest* two-symbol block ending in $f^{(iii)}$. Since there is only one symbol, a_2 , that maps to $f^{(iii)}$, we add a_2 on the left-hand side. We again record the two-symbol parities below each pair of symbols. Since $\pi(a_2 f^{(iii)})$ is again negative, the total parity, recorded on the right, is now $\pi(a_2 f^{(iii)} a_1) = +1$. With this positive parity, the next symbol we seek is the one forming the *largest* two-symbol itinerary ending in a_2 , which is $a_1 a_2$, so a_1 is added on the left. We have thus returned to the symbol a_1 , with positive total parity, and hence

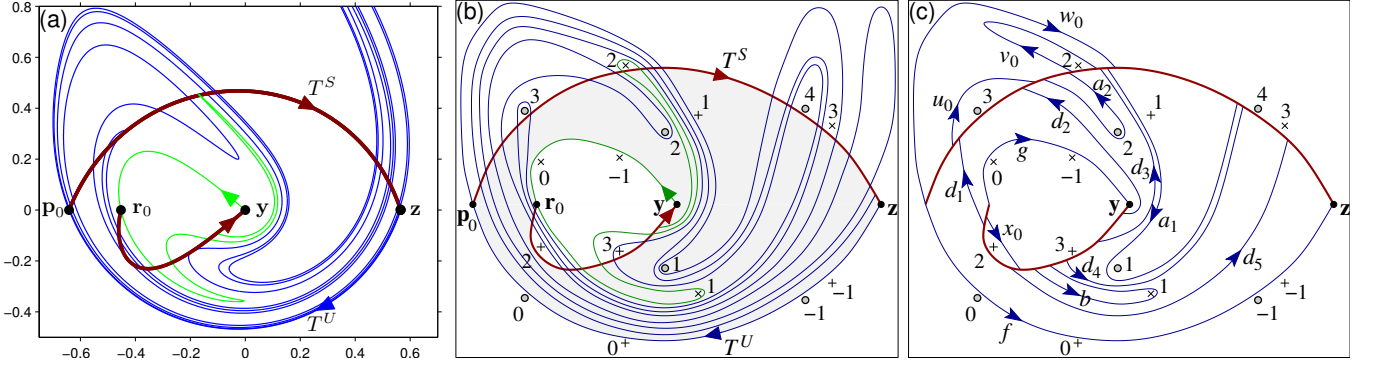


Figure 20: (Color online) (a) A nested trellis for the same map used in Fig. 3. The inner trellis is attached to the fixed point y . (b) A qualitative depiction of Fig. 20a, which shows the topological structure more clearly. There are three sequences of holes depicted by exes, pluses, and circles, and labeled by their iterate number. (c) An illustration of the bridge classes, showing how each winds around the holes.

the pattern must repeat, with the complete itinerary being $\dots(a_2 f^{(iii)} a_1)(a_2 f^{(iii)} a_1) = a_2 f^{(iii)} a_1$.

minimum itinerary ending in a_1 : We again outline the steps.

Step	Constructed Itinerary	Total Parity π
1	$f^{(i)} a_1$ -1	-1
2	$f^{(i)} f^{(i)} a_1$ +1 -1	-1

final itinerary = $\overline{f^{(i)} a_1}$

Since we are trying to minimize the itinerary, the symbol added at step 1 minimizes two-symbol blocks ending in a_1 . As the total parity at step 1 is negative, at step two we look for the symbol which maximizes two-symbol blocks ending in $f^{(i)}$, which is $f^{(i)}$. As total parity at step 2 remains negative, $f^{(i)}$ is repeated forever.

The extreme itineraries for the other symbols are summarized in Table 1. Notice that all of these itineraries begin with one of two periodic sequences $a_1 a_2 f^{(iii)}$ or $f^{(i)}$. The latter is the itinerary of the fixed point z in Fig. 3. The former is the itinerary of a period-three orbit, which lies within the resonance zone and is not an anchor point of the trellis. This orbit is shown in Fig. 19b by the three dots that lie on the partition boundaries for a_1 , a_2 , and $f^{(iii)}$.

From the algorithm for constructing the extreme itineraries, one can immediately see that if $\overline{a_{-p+1} \dots a_{-1} a_0 s_{-n} \dots s_{-1} s}$ is an extreme itinerary for s , then $\overline{a_{-p+1} \dots a_{-1} a_0 s_{-n} \dots s_{-1}}$ is an extreme itinerary for s_{-1} and so forth. This also means that in the process of computing the extreme itinerary for s one also computes one of the two extreme itineraries for all preceding symbols s_{-k} . (In terms of the partition, this means that the unstable boundary of $R_{s_{-k}}$ maps forward across the unstable boundary of $R_{s_{-k+1}}$.)

We can graphically illustrate the relationship between the extreme itineraries in a tree, as shown in Fig. 18. The top nodes contain the periodic starting sequences. Moving down the tree one adds the symbol within each node to the right end of the sequence. In this manner, all extreme itineraries are recovered. Each node also has a “max” or “min” label indicating whether the itinerary ending in that node is a maximum or minimum.

Suppose now that we have determined the itinerary of a boundary interval $\overline{a_{-p+1} \dots a_{-1} a_0 s_{-n} \dots s_{-1} s}$. We next wish to compute the actual boundary interval B with this itinerary. This problem reduces to that of finding the limRoD-bridge A_0 with itinerary $\overline{a_{-p+1} \dots a_{-1} a_0}$, since, as discussed in Sec. 6.2, once we know A_0 , we can propagate it forward to find the interval B . If $\overline{a_{-p+1} \dots a_{-1} a_0}$ is an anchor sequence, then A_0 is simply an anchor limRoD-bridge within the trellis T^U . However, if $\overline{a_{-p+1} \dots a_{-1} a_0}$ is not an anchor sequence, then A_0 is an unstable interval attached to a periodic orbit that is not in the set of anchor points P . In this case, we can approximate A_0 arbitrarily accurately with an interval of W^U . To construct an approximating interval to A_0 , first consider any finite itinerary of the form $a' \dots (a_{-p+1} \dots a_{-1} a_0)^k$. Here the itinerary ends in k repetitions of $a_{-p+1} \dots a_{-1} a_0$ and begins with the symbol a' , which is taken to be an anchor symbol. Since this itinerary begins with an anchor symbol, the corresponding anchor limRoD-bridge A' lies within the trellis T^U , and is thus easy to identify. It is straightforward then to iterate A' forward to construct a limRoD-bridge A_0^k with the itinerary $a' \dots (a_{-p+1} \dots a_{-1} a_0)^k$. The approximant A_0^k converges to A_0 exponentially in k . Once this approximant is found to the desired accuracy, it can be used to construct the desired boundary interval B .

Finally, when computing the interval for a given extreme itinerary, one may find more than one limRoD-bridge with that itinerary, as discussed in Sec. 6.2. Clearly in this case, the boundary interval is the most extreme of these limRoD-bridges with respect to the \blacktriangleleft -order.

Example: For the example introduced in Fig. 3, Fig. 19b plots the five partition rectangles, whose extreme itineraries are in Table 1. Notice that for the symbols a_1 , a_2 , and $f^{(iii)}$, the partition rectangles are

drawn in toward the central stable region, where they are starting to form extended and bent “fingers”. This suggests that the stable region is exerting an influence on the structure of the surrounding chaotic sea, and that this influence has not been fully incorporated into the symbolic dynamics at this stage of resolution. That is, the partition in Fig. 19b has not fully resolved the topological dynamics in the vicinity of the stable region. We shall improve this situation in Sec. 9.

9. Resolving the partition in the vicinity of stable islands

The fingering evident in Fig. 19b is a reflection of the fact that the trellis in Fig. 19a (or equivalently Fig. 3a) has not accurately captured the topology of the dynamics in the vicinity of the stable zone. (For example, the topological entropy computed from the symbolic dynamics in Fig. 14 is less than the true topological entropy of the map.) As pointed out in Ref. [17], we can more accurately describe the topological dynamics in the vicinity of stable islands by including additional homoclinic or heteroclinic tangles attached to unstable periodic orbits near the islands. In the present example, we follow Ref. [17] and expand the trellis T to include a second homoclinic tangle attached to the fixed point \mathbf{y} and surrounding the stable zone, as shown in Fig. 20a. For clarity, Fig. 20b includes a schematic drawing of the expanded trellis. The homotopic lobe dynamics for this trellis was discussed in detail in Ref. [17], and here we summarize the concise dynamics in the top set of equations of Fig. 21. Note that these equations expand slightly on the results of Ref. [17] by incorporating the symbol refinement discussed in Sec. 5.2. (The dedicated reader would benefit from confirming these refined equations.) The refined equations yield the transition graph in Fig. 21, where each directed edge is labeled by the parity of the transition. Figure 20c illustrates a representative curve from each homotopy class. From this illustration, the \blacktriangleleft_f - and \blacktriangleleft_i -ordering of individual symbols can be read off, as recorded in Fig. 21. The orderings of two-symbol blocks in Fig. 21 follows from the technique in Sec. 7, using the concise dynamics and the orderings of individual symbols in Fig. 21. Finally, the method of Sec. 8 uses the ordering of two-symbol blocks to produce the extreme itineraries in Table 2, which are organized into the tree in Fig. 22. From these extreme itineraries, we can compute the partition elements themselves, as shown in Fig. 19d. This partition, with 13 elements, is clearly an improvement over the previous partition to its left, with only 5.

The partition can be further refined if we use a trellis T with a higher density of unstable manifold and which penetrates the inner region of the chaotic sea closer to the stable zone, as shown in Fig. 19e. The corresponding partition, shown in Fig. 19f, exhibits a much higher degree of refinement, with 80 elements, especially in the vicinity of the stable zone. At this point, the symbolic dynamics was complicated enough that the algorithms to extract the homotopic lobe dynamics and to ultimately compute the extreme itineraries were implemented in Matlab, along with the algorithms to numerically compute the

terminal symbol	maximum	minimum
a_1	$\bar{f}a_1fa_1$	$\bar{f}a_1$
b	$\bar{f}a_1d_5^{(ii)}d_3^{(ii)}d_2gb$	$\bar{g}b$
g	\bar{g}	$\bar{f}a_1d_5^{(ii)}d_3^{(ii)}d_2g$
d_4	$\bar{f}a_1fa_1a_2d_1^{(ii)}d_4$	$\bar{f}a_1d_1^{(i)}d_4$
f	\bar{f}	$\bar{f}a_1f$
a_2	$\bar{f}a_1fa_1a_2$	$\bar{f}a_1a_2$
$d_1^{(i)}$	$\bar{f}a_1a_2d_1^{(i)}$	$\bar{f}a_1d_1^{(i)}$
$d_1^{(ii)}$	$\bar{f}a_1fa_1a_2d_1^{(ii)}$	$\bar{f}a_1a_2d_1^{(ii)}$
$d_3^{(i)}$	$\bar{g}bd_3^{(i)}$	$\bar{f}a_1d_1^{(i)}d_4d_3^{(i)}$
$d_3^{(ii)}$	$\bar{f}a_1d_5^{(ii)}d_3^{(ii)}$	$\bar{g}bd_3^{(ii)}$
$d_5^{(i)}$	$\bar{f}a_1a_2d_5^{(i)}$	$\bar{f}a_1d_1^{(i)}d_4d_3^{(i)}d_2d_5^{(i)}$
$d_5^{(ii)}$	$\bar{f}a_1d_5^{(ii)}$	$\bar{f}a_1a_2d_5^{(ii)}$
d_2	$\bar{f}a_1d_5^{(ii)}d_3^{(ii)}d_2$	$\bar{f}a_1d_1^{(i)}d_4d_3^{(i)}d_2$

Table 2: Extreme itineraries for symbolic dynamics in Fig. 21.

partition boundaries themselves.⁸

10. Discussion

This work demonstrates how a trellis, i.e. finite-length intervals of stable and unstable manifolds, can be used to construct a partition of a chaotic phase space, even when the phase space contains islands of stability that substantially influence the dynamics in their vicinity. The partition is constructed from an underlying Markov shift and has the feature that every allowed symbol sequence of the shift has a phase-space trajectory with that itinerary. Furthermore, the level of refinement of the partition, and the accuracy of the shift, depend on the number, length, and density of the stable and unstable intervals used in its construction. Figure 19 illustrates how increasing the density of unstable intervals improves the resolution of the partition.

A key remaining issue is the strategy for selecting and refining the initial trellis itself. We discuss a few approaches. As emphasized previously, to construct the partition, one often must use intervals that are not contained in the original trellis. In the process of computing these intervals, one often finds that they have additional structure (i.e. heteroclinic intersections) that were not predicted by the topology of the original trellis. (This is the reason for using RoD-bridges in the text.) A natural strategy would then be to expand the original trellis with the additional unstable intervals discovered upon construction of the partition. From this expanded trellis, a new refined partition could be computed. This new partition may contain additional structure as well, and the refinement could be repeated. This process could be repeated recursively until either there is no new structure or until any new structure is below some tolerance, characterized, for example, as being smaller than some threshold area in phase space. Though potentially useful, this

⁸Implementation details will be provided elsewhere. Interested parties may contact the author for the code.

Concise dynamics of active symbols

$$M(a_1) = d_5^{(ii)-1} x_0^{-1} d_1^{(i)} u_0 a_2 u_0^{-1} f,$$

$$M(a_2) = d_5^{(i)-1} x_0^{-1} d_1^{(ii)} u_0^{-1} d_1^{(i)-1} x_0 d_5^{(ii)},$$

$$M(d_4) = d_3^{(i)} u_0^{-1} f,$$

$$M(g) = b^{-1} x_0^{-1} g.$$

$$M(d_1^{(k)}) = d_4,$$

$$M(d_2) = g^{-1} x_0 d_5^{(i)},$$

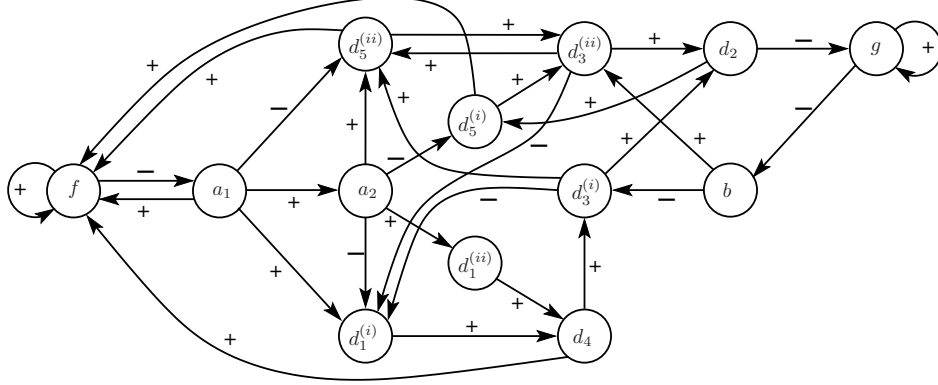
$$M(d_5^{(k)}) = d_3^{(ii)} w_0^{-1} f,$$

$$M(b) = d_3^{(ii)} v_0^{-1} d_3^{(i)-1},$$

$$M(d_3^{(k)}) = d_2 u_0^{-1} d_1^{(i)-1} x_0 d_5^{(ii)},$$

$$M(f) = a_1^{-1} w_0^{-1} f,$$

Transition graph (active symbols only)



◀_i-ordering of symbols (smallest to largest)

$$\leftarrow_i: f^{-1} d_5^{(ii)-1} d_5^{(i)-1} d_4^{-1} a_1^{-1} a_1 d_3^{(ii)-1} d_3^{(i)-1} a_2^{-1} a_2 d_2^{-1} d_1^{(ii)-1} d_1^{(i)-1} f g^{-1} d_2 d_3^{(i)} d_3^{(ii)} d_4 b^{-1} b d_5^{(i)} d_5^{(ii)} d_1^{(i)} d_1^{(ii)} g.$$

◀_f-ordering is obtained by reversing the above ordering and inverting each symbol.

Ordering of two-symbol blocks

$$\begin{aligned} d_2 g &\leftarrow gg \\ d_1^{(i)} d_4 &\leftarrow d_1^{(ii)} d_4 \\ d_4 d_3^{(i)} &\leftarrow b d_3^{(ii)} \end{aligned}$$

$$\begin{aligned} d_3^{(i)} d_2 &\leftarrow d_3^{(ii)} d_2 \\ d_2 d_5^{(i)} &\leftarrow a_2 d_5^{(ii)} \\ b d_3^{(ii)} &\leftarrow d_5^{(i)} d_3^{(ii)} \leftarrow d_5^{(ii)} d_3^{(i)} \end{aligned}$$

$$\begin{aligned} a_1 f &\leftarrow d_4 f \leftarrow d_5^{(i)} f \leftarrow d_5^{(ii)} f \leftarrow f f \\ a_1 d_1^{(i)} &\leftarrow d_3^{(ii)} d_1^{(i)} \leftarrow d_3^{(i)} d_1^{(ii)} \leftarrow a_2 d_1^{(i)} \\ a_2 d_5^{(ii)} &\leftarrow d_3^{(i)} d_5^{(ii)} \leftarrow d_3^{(ii)} d_5^{(i)} \leftarrow a_1 d_5^{(ii)} \end{aligned}$$

Figure 21: Summary of symbolic dynamics for the example in Fig. 20. See Ref. [17] for the derivation of the concise dynamics.

strategy by itself may nevertheless fail to find all topological structures above the desired threshold.

A second strategy would be to start with a rather small and simple homoclinic or heteroclinic trellis, and then recursively expand the trellis by adding in higher and higher iterates of the unstable manifold. Since this manifold is ultimately dense in the chaotic sea, a sufficiently large number of iterates would eventually detect any given topological feature. In practice, one would stop adding new intervals once some tolerance, e.g. some threshold in phase space area, is reached. A difficulty with this approach, however, is that a large number of relatively long intervals may be needed to penetrate into some important areas of phase space (e.g. those near stable islands).

A third strategy, highlighted in Sec. 9, is to directly target the vicinity of stable islands using stable and unstable manifolds that are attached to additional unstable periodic orbits near the islands and that envelope the islands. With a numerically

computed phase space portrait, the larger of these islands can easily be identified visually and unstable orbits between the islands can typically be computed quite quickly. As demonstrated in Fig. 1 and Fig. 19, this is an effective and readily implementable strategy. One drawback of the present implementation is that it can be cumbersome to detect progressively smaller island chains and to add in new stable and unstable branches “by hand”.

The above three strategies are all useful approaches and can be used in combination with one another to produce partitions that capture arbitrarily small features in phase space. A remaining question is how to achieve such fine-scale resolution with maximal efficiency and physical insight. We envision a strategy that starts with a simple trellis capturing the basic large-scale dynamical features. This trellis would then be expanded to include higher and higher iterates of the unstable manifold. As the unstable intervals begin to penetrate the region surround-

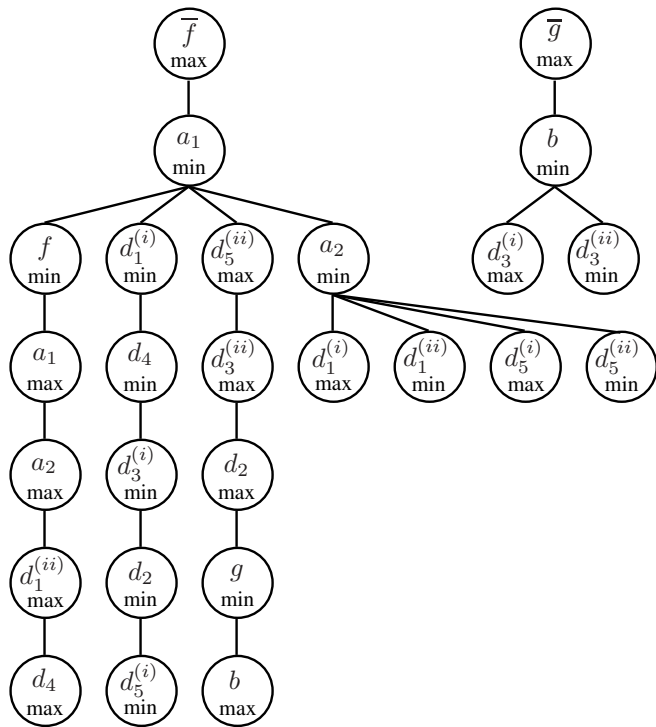


Figure 22: Extreme itinerary tree graphically organizing the itineraries in Table 2.

ing the stable islands, the algorithm would automatically detect the presence of the islands and their associated unstable orbits. These orbits and an initial finite length of their invariant manifolds would then be added to the trellis, and the procedure would continue. As more unstable intervals are added to the trellis, more island chains would be detected and more stable and unstable branches added to the trellis, penetrating closer to the islands. Such an algorithm would necessarily have a tolerance (e.g. based on a threshold in the phase space area) so that any topological feature below this tolerance would not be refined further. Implementing such a strategy efficiently, and in particular detecting when to add new branches to the trellis (as opposed to simply expanding the existing branches), is the subject of ongoing research.

Acknowledgements

This work was supported by NSF grant # PHY-0748828.

References

- [1] J. Guckenheimer, P. Holmes, *Nonlinear oscillations, dynamical systems, and bifurcations of vector fields*, Springer, New York, 1983.
- [2] D. Lind, B. Marcus, *An introduction to symbolic dynamics and coding*, Cambridge University Press, Cambridge, 1995.
- [3] M. C. Gutzwiller, *Chaos in Classical and Quantum Mechanics*, Springer, New York, 1990.
- [4] P. Cvitanović, R. Artuso, R. Mainieri, G. Tanner, G. Vattay, *Chaos: Classical and Quantum*, Niels Bohr Institute, Copenhagen, 2010, ChaosBook.org.

- [5] S. M. Ulam, *A Collection of mathematical problems*, Vol. 8 of Interscience tracts in pure and applied mathematics, Interscience, New York, 1960.
- [6] T.-Y. Li, Finite approximation for the frobenius-perron operator. a solution to Ulam's conjecture, *Journal of Approximation Theory* 17 (2) (1976) 177 – 186.
- [7] E. M. Bollt, T. Stanford, Y.-C. Lai, K. Zyczkowski, What symbolic dynamics do we get with a misplaced partition? : On the validity of threshold crossings analysis of chaotic time-series, *Physica D: Nonlinear Phenomena* 154 (3-4) (2001) 259 – 286.
- [8] J. Milnor, W. Thurston, On iterated maps of the interval, in: *Dynamical systems* (College Park, MD, 1986–87), Vol. 1342 of *Lecture Notes in Math.*, Springer, Berlin, 1988, pp. 465–563.
- [9] R. Gilmore, M. Lefranc, *The Topology of Chaos: Alice in Stretch and Squeezeland*, Wiley-Interscience, 2002.
- [10] P. Grassberger, H. Kantz, Generating partitions for the dissipative Hénon map, *Physics Letters A* 113 (5) (1985) 235 – 238.
- [11] P. Grassberger, H. Kantz, U. Moenig, On the symbolic dynamics of the Henon map, *Journal of Physics A: Mathematical and General* 22 (24) (1989) 5217.
- [12] P. Cvitanović, G. H. Gunaratne, I. Procaccia, Topological and metric properties of Hénon-type strange attractors, *Phys. Rev. A* 38 (3) (1988) 1503–1520.
- [13] F. Christiansen, A. Politi, Generating partition for the standard map, *Phys. Rev. E* 51 (5) (1995) 3811–3814.
- [14] F. Christiansen, A. Politi, Symbolic encoding in symplectic maps, *Nonlinearity* 9 (6) (1996) 1623.
- [15] F. Christiansen, A. Politi, Guidelines for the construction of a generating partition in the standard map, *Physica D* 109 (1997) 32–41.
- [16] C. Jung, A. Emmanouilidou, Construction of a natural partition of incomplete horseshoes, *Chaos* 15 (2005) 023101.
- [17] K. A. Mitchell, The topology of nested homoclinic and heteroclinic tangles, *Physica D* 238 (7) (2009) 737–763.
- [18] K. A. Mitchell, J. B. Delos, A new topological technique for characterizing homoclinic tangles, *Physica D* 221 (2006) 170.
- [19] K. A. Mitchell, J. P. Handley, S. K. Knudson, J. B. Delos, Geometry and topology of escape. II. homotopic lobe dynamics, *Chaos* 13 (2003) 892.
- [20] P. Collins, Dynamics forced by surface trellises, in: *Geometry and topology in dynamics*, Vol. 246 of *Contemp. Math.*, Amer. Math. Soc., Providence, RI, 1999, pp. 65–86.
- [21] P. Collins, Symbolic dynamics from homoclinic tangles, *Int. J. Bifurcation Chaos Appl. Sci. Eng.* 12 (3) (2002) 605–617.
- [22] P. Collins, Dynamics of surface diffeomorphisms relative to homoclinic and heteroclinic orbits, *Dyn. Syst.* 19 (1) (2004) 1–39.
- [23] P. Collins, Entropy-minimizing models of surface diffeomorphisms relative to homoclinic and heteroclinic orbits, *Dyn. Syst.* 20 (4) (2005) 369–400.
- [24] P. Collins, Forcing relations for homoclinic orbits of the Smale horseshoe map, *Exp. Math.* 14 (1) (2005) 75–86.
- [25] M. Bestvina, M. Handel, Train tracks and automorphisms of free groups, *Ann. Math.* 135 (1992) 1.
- [26] M. Bestvina, M. Handel, Train-tracks for surface homeomorphisms, *Topology* 34 (1995) 109.
- [27] R. W. Easton, Trellises formed by stable and unstable manifolds in the plane, *Trans. Am. Math. Soc.* 294 (1986) 719.
- [28] R. Easton, *Geometric Methods for Discrete Dynamical Systems*, Oxford University Press, New York, 1998.
- [29] V. Rom-Kedar, Transport rates of a class of two-dimensional maps and flows, *Physica D* 43 (1990) 229.
- [30] V. Rom-Kedar, Homoclinic tangles-classification and applications, *Nonlinearity* 7 (1994) 441.
- [31] B. Ruckerl, C. Jung, Scaling properties of a scattering system with an incomplete horseshoe, *J. Phys. A* 27 (1994) 55.
- [32] B. Ruckerl, C. Jung, Hierarchical structure in the chaotic scattering off a magnetic dipole, *J. Phys. A* 27 (1994) 6741.
- [33] C. Lipp, C. Jung, A degenerate bifurcation to chaotic scattering in a multicentre potential, *J. Phys. A* 28 (1995) 6887.
- [34] M. Dellnitz, O. Junge, *Handbook of Dynamical Systems*, Vol. 2, Elsevier, Amsterdam, 2002, Ch. 5, pp. 221–270.
- [35] S. Wiggins, *Chaotic Transport in Dynamical Systems*, Springer-Verlag, New York, 1992.

- [36] P. Collins, B. Krauskopf, Entropy and bifurcations in a chaotic laser, *Phys. Rev. E* 66 (5) (2002) 056201.
- [37] V. Rom-Kedar, S. Wiggins, Transport in two-dimensional maps, *Archive for Rational Mechanics and Analysis* 109 (1990) 239.
- [38] K. A. Mitchell, J. P. Handley, B. Tighe, A. Flower, J. B. Delos, Chaos-induced pulse trains in the ionization of hydrogen, *Phys. Rev. Lett.* 92 (2004) 073001.
- [39] K. A. Mitchell, J. P. Handley, B. Tighe, A. Flower, J. B. Delos, Analysis of chaos-induced pulse trains in the ionization of hydrogen, *Phys. Rev. A* 70 (2004) 043407.
- [40] P. Collins, K. Mitchell, Graph duality in surface dynamics, in preparation.